View Article Online / Journal Homepage / Table of Contents for this issue

Multi-path variational transition state theory for chemical reaction rates of complex polyatomic species: ethanol + OH reactions†

Jingjing Zheng and Donald G. Truhlar*

Received 29th January 2012, Accepted 29th February 2012
DOI: 10.1039/c2fd20012k

Published on 29 February 2012 on http://pubs.rsc.org | doi:10.1039/C2FD20012K
Downloaded by University of Minnesota - Twin Cities on 20 January 2013

Complex molecules often have many structures (conformations) of the reactants and the transition states, and these structures may be connected by coupled-mode torsions and pseudorotations; some but not all structures may have hydrogen bonds in the transition state or reagents. A quantitative theory of the reaction rates of complex molecules must take account of these structures, their coupled-mode nature, their qualitatively different character, and the possibility of merging reaction paths at high temperature. We have recently developed a coupled-mode theory called multi-structural variational transition state theory (MS-VTST) and an extension, called multi-path variational transition state theory (MP-VTST), that includes a treatment of the differences in the multi-dimensional tunneling paths and their contributions to the reaction rate. The MP-VTST method was presented for unimolecular reactions in the original paper and has now been extended to bimolecular reactions. The MS-VTST and MP-VTST formulations of variational transition state theory include multi-faceted configuration-space dividing surfaces to define the variational transition state. They occupy an intermediate position between single-conformation variational transition state theory (VTST), which has been used successfully for small molecules, and ensemble-averaged variational transition state theory (EA-VTST), which has been used successfully for enzyme kinetics. The theories are illustrated and compared here by application to three thermal rate constants for reactions of ethanol with hydroxyl radical—reactions with 4, 6, and 14 saddle points.

I. Introduction

The progress in density functionals that allows a quantitative treatment of the potential energy surfaces of complex reactions[1–3] places new demands on reaction rate theory for maintaining a high level of accuracy in the treatment of the dynamics. Complex molecules often have many structures (conformations) of the reactants and the transition states, and these structures may be connected by coupled-mode torsions and pseudorotations; some but not all structures may have hydrogen bonds in the transition state or reagents. A quantitative theory of the reaction rates of complex molecules must take account of these structures, their coupled-mode nature, their qualitatively different character, and the possibility of merging reaction paths at high temperature.

Department of Chemistry and Supercomputing Institute, University of Minnesota, Minneapolis, Minnesota 55455-0431. E-mail: truhlar@umn.edu

† Electronic supplementary information (ESI) available: Cartesian coordinates of optimized geometries. See DOI: 10.1039/c2fd20012k

View Article Online

Published on 29 February 2012 on http://pubs.rsc.org | doi:10.1039/C2FD20012K
Downloaded by University of Minnesota - Twin Cities on 20 January 2013

Transition state theory[4,5] (TST) provides an efficient way to obtain thermal reaction rate constants. Transition state theory has a long history, and it is widely understood to be a very general theory of reaction rates.[4–10] Early doubts about the reasonableness of its assumptions have been largely erased by incorporating variational transition states and multidimensional tunneling approximations and by comparing the results to accurate quantum mechanical calculations on simple reactions and to experiment, especially kinetic isotope effects, for a variety of processes, both simple and complex.[9–13] Advances in electronic structure theory have allowed one to obtain accurate enough potential energy surfaces that the hope of calculating absolute reaction rates is sometimes achieved for simple systems and is becoming within reach for more and more complicated systems. Practical methods have been proposed for defining sequences of generalized transition states and optimizing variational transition states within the sequences.[14–25] At this stage of theoretical development, the chief sources of concern, aside from the accuracy of the potential energy surface, when applying transition state theory to practical problems are issues such as the choice of reaction coordinate, the treatment of anharmonicity, and ensemble averaging over all contributing structures of the reactants and the generalized transition states.

Reactions of small molecules without torsions often have only a single conformation of the reactants and a single conformation of the transition state. Textbook presentations of transition state theory are often limited to this case, and the relevant partition functions are often treated as products of separable translational, rotational, vibrational, and electronic contributions, with the vibrational modes treated independently of each other and of rotation.[26] At the other extreme are complex reactions in solution or in enzymes. Here one must deal directly with free energies and free energies of activation that correspond to essentially uncountable numbers of conformations of the reagents, solvent molecules, and possibly catalysts. Intermediate between these extremes are gas-phase reactions of molecules with torsions. Here, as compared to small-molecule kinetics, there can be an appreciable conformational contribution to the free energies, and some vibrational modes may be strongly coupled to one another and to overall rotation. However, as compared to reactions in liquids or in enzymes, the number of conformations, although large, is countable. We have recently developed two formulations[27,28] of variational transition state theory, including multidimensional tunneling contributions, that are applicable to the case of gas-phase molecules with nonseparable torsions. We presented them in their most primitive form, and we applied the first[27] to reactions with up to 262 distinguishable conformations of the transition state[29] and the second to a reaction with four distinguishable conformations of the transition state.[28]

The first new formulation of TST is a coupled-mode theory called multi-structural variational transition state theory[27] (MS-VTST), and the second, multi-path VTST[28] (MP-VTST), extends it to multiple reaction paths to include a more complete treatment of the differences in the multi-dimensional tunneling paths and their contributions to the reaction rate. The new theories use a multi-faceted configuration-space dividing surface to define the variational transition state. Note that MP-VTST and MS-VTST both include the contribution of all the reaction paths to the total reactive flux, but MS-VTST does this in a more approximate way. MS-VTST is a special case of MP-VTST. MS-VTST has been presented elsewhere[27] and applied to unimolecular[27,28] and bimolecular reactions.[30,31] The MP-VTST was presented for and applied to unimolecular reactions.[28] Here we present MP-VTST for bimolecular reactions, explain the additional approximations that reduce it to MS-VTST, and then apply both MP-VTST and MS-VTST to three reactions.

We will also discuss the challenges in applying TST to calculate thermal rate constants accurately, especially for complex systems. A key challenge is interfacing methods for calculating potential energy surfaces to dynamical steps requiring a semi-global potential energy surface, such as the treatment of variational effects, quantum effects, and anharmonicity. Some calculations in the literature have

 This journal is © The Royal Society of Chemistry 2012

View Article Online

achieved good agreement with experimental data without considering all sources of these important effects or by using inaccurate potential energy surfaces because the agreement between experiments and calculations is sometimes achieved by error cancellation in the calculations, but to make theory reliably predictive one cannot rely on error cancellation, and we need to understand the possible sources of error and the best available strategies to mitigate these errors.

The reactions studied in the present work are three hydrogen abstraction reactions of the various sites of ethanol with hydroxyl radicals,

$$CH_3CH_2OH + OH \rightarrow CH_3CHOH + H_2O \quad \text{(R1a)}$$

$$CH_3CH_2OH + OH \rightarrow CH_2CH_2OH + H_2O \quad \text{(R1b)}$$

$$CH_3CH_2OH + OH \rightarrow CH_3CH_2O + H_2O \quad \text{(R1c)}$$

These reactions are important elementary steps in biofuel combustion and have been extensively studied experimentally[32–41] and theoretically.[40,42,43] The overall reaction rate constant, k_1, is the sum of k_{1a}, k_{1b}, and k_{1c}, and the IUPAC[44] recommendation for this quantity is $6.70 \times 10^{-18}\ T^2\ \exp(511/T)$ cm^{3}molecule^{-1}s^{-1} over the temperature range 216–599 K. The branching ratios are less well established.[39] Although these reactions have been studied by several groups using TST,[40,42,43] there is still much to learn, and in the present work we will present a more detailed analysis and discussion of these reactions based on our newly developed multi-path and multi-structural versions of VTST, and we will use these reactions as examples to show the challenges in obtaining accurate thermal rate constants of complex polyatomic systems using state-of-art electronic structure and dynamics methods.

II. Computational methods

II. A. Electronic structure methods

The conformational structures of ethanol, the hydroxyl radical, and the saddle points are optimized by various density functionals including M08-HX,[45] M08-SO,[45] M05-2X,[46] and M06-2X.[47] The 6-31+G(d,p) basis set is used for all geometry optimizations and for the straight direct dynamics calculations except that the ma-TZVP[48] basis set is used for M08-HX and M08-SO calculations for R1a to test the sensitivity to basis set.

The first grid used for density functional integrations is a pruned grid based on 99 radial shells around each atom and 974 angular points in each shell. This grid is used for the optimization and frequency calculation for all the stationary points and for the reaction paths of R1a and R1c. The reaction paths for R1b require a finer grid, and we used a grid that has 96 radial shells around each atom and a spherical product angular grid having 32 θ points and 64 φ points in each shell.

The best estimate (BE) classical barrier height is obtained by a two-step procedure. The first step is to estimate the complete basis set (CBS) limit of the coupled-cluster singles and doubles method with quasiperturbative inclusion of connected triples (CCSD(T)).[49] The second step is to add a finite basis set (FBS) correction for a higher-level (HL) treatment of electron correlation energy. Thus

$$V^{\ddagger}_{BE} = V^{\ddagger}_{CBS}(CCSD(T)) + \Delta V^{\ddagger}_{FBS} \quad (1)$$

$$\Delta V^{\ddagger}_{FBS} = V^{\ddagger}(CCSDT(2)_Q/FBS) - V^{\ddagger}(CCSD(T)/FBS) \quad (2)$$

Published on 29 February 2012 on http://pubs.rsc.org | doi:10.1039/C2FD20012K
Downloaded by University of Minnesota - Twin Cities on 20 January 2013

View Article Online

where $V^{\ddagger}$ denotes the classical barrier height. Usually the CBS limit is obtained by extrapolating a few finite basis set results, but here we used a more efficient method, namely CCSD(T)-F12b[50,51] with a may-cc-pVQZ[52] basis set, to approximate the CCSD(T)/CBS limit. We also calculated CCSD(T)-F12a/aug-cc-pVTZ energies to check the convergence with respect to the basis set.

The FBS correction accounts for the effect of higher excitations by using the CCSDT(2)$_Q$[53] method with a finite basis set. The basis set for use in eqn (2) can be smaller than that for eqn (1) because the higher-level corrections show faster basis set convergence. The finite basis set used in eqn (2) is the maug-cc-pVDZ[54] basis set. To check this assumption, we also calculate $\Delta V^{\ddagger}_{HL}$ by using a smaller basis set, cc-pVDZ.

Restricted open-shell Hartree–Fock orbitals are used for all the coupled cluster calculations. In all coupled cluster calculations (CCSD(T), CCSD(T)-F12a, CCSD(T)-F12b, and CCSDT(2)$_Q$), correlation of core electrons is not included.

To gauge the importance of multi-reference character in the stationary-point electronic wave functions, we computed the T_1 diagnostic.[55] It has been suggested that significant multi-reference character, and hence a concomitant higher than usual inaccuracy of CCSD(T) calculations, is indicated by a T_1 diagnostic of 0.02 or greater for closed-shell systems[55] and by a T_1 diagnostic of 0.045 or greater for open-shell systems.[56–58]

For computing vibrational partition functions, all Hessians and force constants (in either internal or Cartesian coordinates) are multiplied by λ^2_{ZPE}, where λ_{ZPE} is a previously determined scale factor[59] that, when the frequencies computed from scaled Hessians are used in the harmonic oscillator (HO) formula, should make the zero-point energy more accurate. The scale factor accounts for systematic errors in the electronic structure method but also, significantly, for the difference (on average) between zero-point energies computed by the HO formula and those including anharmonicity. For this reason, when results given below are labeled as HO or local harmonic (LH), the label and the language refer to the use of the HO formulas; the results themselves are quasiharmonic because of the use of scaling to account (approximately) for anharmonicity. But this mainly includes the anharmonicity in the high-frequency modes because it is the high-frequency modes that dominate the zero-point energy. Anharmonicity due to low-frequency torsions is accounted for by the method discussed in the next subsection.

All the density functional calculations were performed by the *Gaussian 09*[60] package with the *MNGFM* version 5.1[61] module. The CCSD(T)-F12a/b calculations were carried out by the *Molpro*[62] program, and the *NWChem*[63] program was used for CCSDT(2)$_Q$ calculations.

II. B. Partition functions

Ethanol and the transition states of the three reactions each have multiple conformational structures (minima or saddle points, respectively, on the potential energy surface) caused by internal rotations (torsions). We will treat the anharmonicity associated with these torsions by the multi-structural method including torsional anharmonicity[64] (MS-T). In the MS-T calculations, the translational partition function and electronic partition function are separable from the conformational–rotational–vibrational partition function.

The MS-T method can be applied to both stable species and transition states. We will label a general species as α, which can be a reactant (R_i with $i = 1$ or 2) or the saddle point ‡. A reactant has F vibrational modes, where F is the number of internal coordinates, and a transition state, being a hypersurface dividing reactants from products, has only $F - 1$ vibrations. In general, let j label the distinguishable conformational structures of a species, and let J be the total number of such conformational structures. We will use k and K to denote the structure number and number of structures when we are specifically referring only to the transition state. A

Published on 29 February 2012 on http://pubs.rsc.org | doi:10.1039/C2FD20012K
Downloaded by University of Minnesota - Twin Cities on 20 January 2013

 This journal is © The Royal Society of Chemistry 2012

View Article Online

transition state with K structures is a multifaceted dividing surface with K facets. Because we use curvilinear coordinates,[17] facet k is a curved hypersurface locally orthogonal to the reaction path through saddle point k, as shown in Fig. 1. We will let U_j^α denote the equilibrium potential energy of structure j; for transition states it is the lowest potential energy in facet k. The structure with the lowest value of U_j^α or U_k^α for a given species α is labeled $j = 1$ or $k = 1$, and U_1^α is set equal to zero. Then all other U_j^α are measured with respect to U_1^α. Throughout the entire article all partition functions for species α are calculated with the zero of energy at U_1^α. We will denote the (zero-point-inclusive) ground-state energy of structure j as $\tilde{U}_j^\alpha$.

The conformational–rotational–vibrational partition function is calculated as

$$Q_{\text{con-rovib}}^{\text{MS-T},\,\alpha} = \sum_{j=1}^{J} Q_j^{\text{S},\,\alpha} \tag{3}$$

where $Q_j^{\text{S},\alpha}$ is the contribution of structure j of species α and is given by[64]

$$Q_j^{\text{S},\,\alpha} = Q_{\text{rovib},j}^{\text{SS-HO},\,\alpha} Z_j^\alpha \prod_{\tau=1}^{t_\alpha} f_{j,\tau}^\alpha \tag{4}$$

where t_α is the number of torsions in species α, Z_j^α is a factor for guiding the MS-T scheme to the correct high-temperature limit (within the parameters of the model), $f_{j,\tau}^\alpha$ is a torsional anharmonicity factor based on the internal coordinates, which in conjunction with Z_j^α adjusts the harmonic partition function of structure j for the presence of the torsional motion τ, and the single-structure (SS) rotational-vibrational partition function of structure j using the harmonic oscillator approximation is

$$Q_{\text{rovib},j}^{\text{SS-HO},\alpha} = Q_j^{\text{rot},\alpha} \exp(-U_j^\alpha / k_{\text{B}} T) Q_j^{\text{HO},\alpha} \tag{5}$$

where $Q_j^{\text{rot},\alpha}$ is classical rotational partition function of structure j, k_{B} is Boltzmann's constant, T is temperature, and $Q_j^{\text{HO},\alpha}$ is the local-harmonic-oscillator vibrational partition function calculated at structure j.

We define the MS-T torsional anharmonicity factor for each species as

$$F^{\text{MS-T},\,\alpha} = \frac{Q_{\text{con-rovib}}^{\text{MS-T},\,\alpha}}{Q_{\text{rovib},\,1}^{\text{SS-HO},\,\alpha}} \tag{6}$$

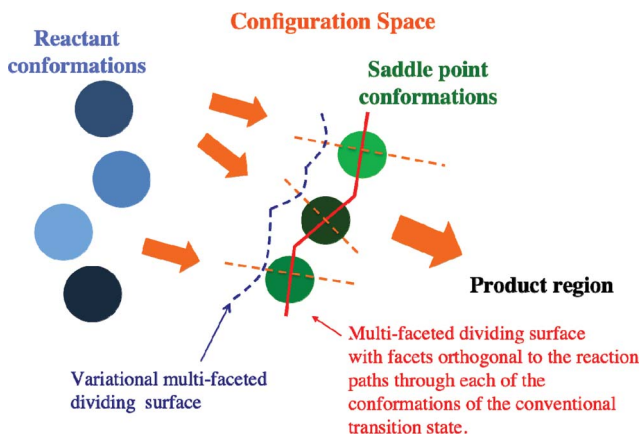

Fig. 1 Multi-faceted dividing surfaces: conventional transition state in red; variational transition state in blue.

Published on 29 February 2012 on http://pubs.rsc.org | doi:10.1039/C2FD20012K
Downloaded by University of Minnesota - Twin Cities on 20 January 2013

View Article Online

where $Q^{SS-HO,\alpha}_{rovib,1}$ is the single-structure rotational-vibrational partition function calculated at the global minimum (structure 1 by definition). Torsional anharmonicity has two aspects. First, the torsions usually generate multiple structures. Second, low barriers along the torsional potential energy profiles mean that the contributions of the structures cannot simply be added together as independent quasiharmonic oscillators, but rather one must account for the merging of the wells as the available energy exceeds the torsional barriers. To separate the effects of multiple-structure anharmonicity, $F^{MS,\alpha}$, from torsional-potential anharmonicity, $F^{T,\alpha}$, we write eqn (6) as

$$F^{MS-T,\alpha} = F^{MS,\alpha}F^{T,\alpha} \tag{7}$$

where

$$F^{MS,\,\alpha} = \frac{Q^{MS-LH,\,\alpha}_{con-rovib}}{Q^{SS-HO,\,\alpha}_{rovib,\,1}} \tag{8}$$

$$F^{T,\,\alpha} = \frac{Q^{MS-T,\,\alpha}_{con-rovib}}{Q^{SS-LH,\,\alpha}_{rovib,\,1}} \tag{9}$$

We define a reaction torsional anharmonicity factor for a bimolecular reaction as

$$F^{MS-T} = \frac{F^{MS-T,\ddagger}}{F^{MS-T,React1}F^{MS-T,React2}} \tag{10}$$

where React1 and React2 are the two reactants of a bimolecular reaction. For the reactions studied in the present work, the OH radical has no torsion so that $F^{MS-T,OH} = 1$, and the torsional anharmonicity activation factor can be written as

$$F^{MS-T} = \frac{F^{MS-T,\ddagger}}{F^{MS-T,\,ethanol}} \tag{11}$$

The MS-T partition functions were calculated by the *MSTor*[65,66] program.

The overall partition function of species α is obtained by multiplying $Q^{MS-T,\alpha}_{con-rovib}$ by the electronic partition function Q^{α}_{elec} and the translational partition function.

II. C. Dynamics: MP-VTST

First we establish notation by considering single-structure VTST, which can be written as

$$k^{VTST} = \frac{k_B T}{h}\frac{Q^{\ddagger}_{elec}}{\Phi^{R}_{trans}\prod_{i=1}^{2} Q^{R_i}_{elec}Q^{SS-HO,\,R_i}_{con-rovib,\,1}}\exp\left(-V^{\ddagger}/k_B T\right)\kappa\Gamma Q^{SS-HO,\,\ddagger}_{con-rovib,\,1} \tag{12}$$

where h is Planck's constant; Φ^{R}_{trans} is a relative translational partition function per volume of the two reactants; $V^{\ddagger}$ is the classical barrier height, that is, the potential energy of the lowest-energy saddle point relative to the lowest reactant; κ is a tunneling transmission coefficient that accounts multidimensional tunneling and nonclassical reflection; and Γ is a recrossing transmission coefficient given by the ratio of the flux through the dynamical bottleneck along the reaction path and the flux through the conventional transition state dividing surface at saddle point $k = 1$. Note that all quantities in eqn (12) except k_B, h, and $V^{\ddagger}$ depend on temperature, but dependence on temperature is not shown as an argument in this article. When eqn (12) is applied with κ set equal to unity, the result is called canonical variational

Downloaded by University of Minnesota - Twin Cities on 20 January 2013
Published on 29 February 2012 on http://pubs.rsc.org | doi:10.1039/C2FD20012K

 This journal is © The Royal Society of Chemistry 2012

View Article Online

theory (CVT), and when it is applied with a multidimensional tunneling (MT) approximation, it is called CVT/MT where MT can be ZCT, SCT, LCT, μOMT, or LAT (denoting respectively the zero-curvature tunneling approximation,[67] the small-curvature tunneling approximation,[68] the large-curvature tunneling approximation,[69–72] the microcanonically optimized multidimensional tunneling approximation,[72] and the least-action tunneling approximation[73,74]). The CVT result is sometimes called quasiclassical to denote that quantum effects are included on the bound motions of the transition state but not on the reaction coordinate.

The meaning of the recrossing coefficient Γ is illustrated by writing eqn (12) as

$$k^{\mathrm{VTST}} = \frac{k_{\mathrm{B}}T}{h}\frac{Q^{\ddagger}_{\mathrm{elec}}}{\Phi^{\mathrm{R}}_{\mathrm{trans}}\prod_{i=1}^{2}Q^{\mathrm{R}_i}_{\mathrm{elec}}Q^{\mathrm{SS-HO,R}_i}_{\mathrm{con\text{-}rovib,1}}}\exp\left(-V^{\ddagger}/k_{\mathrm{B}}T\right)\kappa Q^{\mathrm{SS-HO,\ VTS}}_{\mathrm{con-rovib,\ 1}} \tag{13}$$

where VTS denotes that the partition function is evaluated not at the saddle point but rather at the canonical variational transition state; thus we say that Γ accounts for variational effects. In particular, Γ is the special case with $k = 1$ of

$$\Gamma_k = \frac{\exp(-\max_s G_{T,k}(s)/RT)}{\exp\left(-G^{\ddagger}_{T,k}/RT\right)} \tag{14}$$

where $G_{T,k}$ is the molar generalized free energy of activation[75–77] at temperature T and location s along the minimum-energy path (MEP) through saddle point k, s is the signed distance from saddle point k along that path, $G^{\ddagger}_{T,k}$ is the value of $G_{T,k}$ at $s = 0$, and R is the gas constant.

We account for quantum mechanical effects on the reaction coordinate motion by the transmission coefficient κ. There are two kinds of primary quantum mechanical effects on reaction coordinate motion. First, systems with an energy below the effective barrier height may tunnel through the barrier. Second, systems with energies above the effective barrier, which would be transmitted with unit probability if reaction-coordinate motion were governed by classical mechanics, may be reflected by scattering off the barrier; this is a kind of diffraction, and we call it nonclassical reflection. Because tunneling is usually more important than nonclassical reflection (because the Boltzmann weighting is larger at tunneling energies than at energies above the barrier), we usually call κ the tunneling transmission coefficient. In MS-VTST and MP-VTST, we treat κ by the ground-state tunneling approximation introduced[15,75] in the single-structure version of the theory. In general notation, κ is the special case with $k = 1$ of

$$\kappa_k = \frac{\int_0^{\infty} dEP_k(E)\exp(-E/k_{\mathrm{B}}T)}{\int_0^{\infty} dEP_k^{\mathrm{QC}}(E)\exp(-E/k_{\mathrm{B}}T)} \tag{15}$$

where E is the energy of reaction-coordinate motion, P_k is the quantal probability of transmission from reactants to products in the ground-vibrational state along reaction path k (which is the reaction path through saddle point k), and P_k^{QC} is the approximation to P_k implied by quasiclassical CVT. Therefore P_k^{QC} is a Heaviside step function at $E = \tilde{U}_k^{\mathrm{VTS}}$, which yields

$$\kappa_k = \int_0^{\infty} dEP_k(E)\exp\left[-\left(E-\tilde{U}_k^{\mathrm{VTS}}\right)\Big/k_{\mathrm{B}}T\right] \tag{16}$$

where $\tilde{U}_k^{\mathrm{VTS}}$ is the zero-point-inclusive energy $\tilde{U}_k$ at the maximum generalized free energy of activation determined in eqn (14), and where

$$\tilde{U}_k = V_k(s) + \varepsilon_k^G(s) \tag{17}$$

Published on 29 February 2012 on http://pubs.rsc.org | doi:10.1039/C2FD20012K
Downloaded by University of Minnesota - Twin Cities on 20 January 2013

View Article Online

Published on 29 February 2012 on http://pubs.rsc.org | doi:10.1039/C2FD20012K
Downloaded by University of Minnesota - Twin Cities on 20 January 2013

where V_k and ε_k^G are respectively the potential energy and zero-point vibrational energy along path k. Note that $\tilde{U}_k^{\mathrm{VTS}}$ depends on T because the location of the CVT transition state depends on T. Let V_k^{AG} denote the maximum zero-point-inclusive energy along reaction path k. Then we can note that κ_k differs from unity for three reasons: (i) because P_k is larger than zero for at $E_0 \leq E \leq V_k^{\mathrm{AG}}$ (where E_0 is the quantum threshold energy), which is called tunneling, (ii) because P_k is smaller than unity for $E > V_k^{\mathrm{AG}}$, which is called nonclassical reflection, and (iii) because sometimes $\tilde{U}_k^{\mathrm{VTS}} \neq V_k^{\mathrm{AG}}$, which causes vibrationally adiabatic classical reflection for $\tilde{U}_k^{\mathrm{VTS}} < E < V_k^{\mathrm{AG}}$. Of these three, tunneling is usually the most significant, and so we often call κ_k a tunneling transmission coefficient. It will be convenient for the discussion in Section II. D. to label the lowest-energy V_k^{AG} as V_a^{AG}. Note that the quantum threshold energy E_0 is the lowest energy at which it is possible to have tunneling, and it is $\max[\tilde{U}_1(s=-\infty), \tilde{U}_1(s=\infty)]$ for a bimolecular reaction.

We can combine the recrossing and tunneling effects by defining a generalized transmission coefficient as

$$\gamma_k = \kappa_k \Gamma_k \tag{18}$$

where Γ_k is a recrossing transmission coefficient given by the ratio of the flux through the dynamical bottleneck along path k and flux through the conventional transition state dividing surface at saddle point k.

Next we consider multi-path variational transition state theory with multidimensional tunneling (MT) for calculating the reaction rate constants. The general idea is illustrated in Fig. 1. The facets of a multi-faceted dividing surface are orthogonal the reaction paths through each of the conformations of the transition state. For a bimolecular reaction, the full MP-VTST rate constant at temperature T is

$$k^{\mathrm{MP-VTST/MT}} = \frac{k_B T}{h} \frac{Q_{\mathrm{elec}}^{\ddagger}}{\Phi^{\mathrm{MS\text{-}T,R}}} \exp\left(-V^{\ddagger}/k_B T\right) \sum_{k=1}^{K} \kappa_k \Gamma_k Q_k^{\mathrm{S},\ddagger} \tag{19}$$

where $\Phi^{\mathrm{MS-T,R}}$ is the reactant partition function per unit volume in the center-of-mass frame given by

$$\Phi^{\mathrm{MS-T,R}} = \Phi_{\mathrm{trans}}^{\mathrm{R}} \prod_{i=1}^{2} Q_{\mathrm{elec}}^{\mathrm{R}_i} Q_{\mathrm{con-rovib}}^{\mathrm{MS-T,R}_i} \tag{20}$$

Without any additional approximations, we can rearrange eqn (19) as follows:

$$k^{\mathrm{MP-VTST/MT}} = \langle \gamma \rangle F^{\mathrm{MS-T}} k^{\mathrm{SS-TST}} \tag{21}$$

where $k^{\mathrm{SS\text{-}TST}}$ is the single-structure conventional transition state rate constant in the harmonic approximation:

$$k^{\mathrm{SS\text{-}TST}} = \frac{k_B T}{h} \frac{Q_{\mathrm{elec}}^{\ddagger} Q_{\mathrm{rovib},1}^{\mathrm{SS\text{-}HO},\ddagger}}{\Phi^{\mathrm{SS\text{-}HO,R}}} \exp\left(-V^{\ddagger}/k_B T\right) \tag{22}$$

and where we have defined

$$\Phi^{\mathrm{SS-HO,R}} = \Phi_{\mathrm{trans}}^{\mathrm{R}} \prod_{i=1}^{2} Q_{\mathrm{elec}}^{\mathrm{R}_i} Q_{\mathrm{rovib},1}^{\mathrm{SS\text{-}HO,R}_i} \tag{23}$$

and

$$\langle \gamma \rangle = \frac{\sum_{k=1}^{K} \kappa_k \Gamma_k Q_k^{\mathrm{S},\ddagger}}{\sum_{k=1}^{K} Q_k^{\mathrm{S},\ddagger}} \tag{24}$$

 This journal is © The Royal Society of Chemistry 2012

View Article Online

where the latter may be called an averaged generalized transmission coefficient. In our original application[28] we made the approximation of replacing $Q_k^{S,\ddagger}$ by $Q_{\text{rovib},k}^{\text{SS-OH},\ddagger}$ in eqn (24), but there is no good reason to do that, so here and in the future we will use eqn (24). We also noted that one could replace the full average of eqn (24) by a partial average:

$$\langle\gamma\rangle_P = \frac{\sum_{k=1}^{P} \kappa_k \Gamma_k Q_k^{S,\ddagger}}{\sum_{k=1}^{P} Q_k^{S,\ddagger}} \tag{25}$$

where $P < K$.

Note that we have factored the rate constant into a single-structure local harmonic rate constant times a correction, where we will substitute a quasiharmonic treatment for the harmonic one. Alternatively, although not done here, one could factor the rate constant into a single-structure rate constant that takes some account of torsions times a correction.

When we apply MP-VTST with all κ_k equal to unity, we call the result MP-CVT. When κ_k is included, the result is called MP-CVT/MT, for example, MP-CVT/SCT.

If we set the averaged generalized transmission coefficient to unity, eqn (19) is reduced to the multi-structural conventional transition state theory (MS-TST) rate constant without tunneling:

$$k^{\text{MS-TST}} = F^{\text{MS-T}} \frac{k_B T}{h} \frac{Q_{\text{elec}}^{\ddagger} Q_{\text{rovib,l}}^{\text{SS-HO},\ddagger}}{\Phi^{\text{MS-T,R}}} \exp\left(-V^{\ddagger}/k_B T\right) \tag{26}$$

The single-structure canonical variational theory rate constant is

$$k^{\text{SS-CVT}} = \Gamma_1 k^{\text{SS-TST}} \tag{27}$$

In some cases, it is a good approximation to approximate $\langle\gamma\rangle$ using a single reaction path. This would be the case, for example, if all the Γ_k and κ_k have similar values and therefore one path can be used to represent all the paths. Another case where this approximation would be good is when $Q_1^{S,\ddagger}$ is much larger than all the other $Q_k^{S,\ddagger}$ such that flux along the lowest-energy path dominates the reaction. The lowest-energy saddle point usually has a larger $Q_k^{S,\ddagger}$ than any of the other transition state structures, especially at low temperature where the κ_k differ most significantly from unity. If we set $P = 1$ in eqn (25), the MP-VTST/MT rate constant is reduced to the MS-VTST/MT rate constant[27]

$$k^{\text{MS-VTST}} = \Gamma_1(T)\kappa_1(T) \frac{k_B T}{h} \frac{Q_{\text{elec}}^{\ddagger} Q_{\text{con-rovib}}^{\text{MS-T},\ddagger}}{\Phi^{\text{MS-T,R}}} \exp\left(-V^{\ddagger}/k_B T\right) \tag{28}$$

We previously pointed out[27,28] that when one takes $P = 1$, one can use any representative structure of the transition state, not necessarily the lowest-energy one (as done here); the changes to the formulas are straightforward. If we set $\Gamma_1 = \kappa_1 = 1$ and evaluate the conformational-rovibrational partition functions by the local harmonic[28,65] approximation, then eqn (28) reduces to eqn (17) of an earlier paper.[78]

Finally we consider the calculation of Γ_k and κ_k. The calculation of these quantities requires the calculation of a reaction path through saddle point k. We calculate these quantities using the methods previously developed[79] for SS-CVT/MT calculations, in particular, using the quasiharmonic approximation defined in subsection II. A.

In the present work, we calculated κ_k using the small-curvature tunneling[68] (SCT) approximation. The calculation of Γ_k, κ_k, and $k^{\text{SS-TST}}$ are carried out using the *POLYRATE*[80] program, and the calculation of $Q_k^{S,\ddagger}$ was carried out with the *MSTor*

Published on 29 February 2012 on http://pubs.rsc.org | doi:10.1039/C2FD20012K
Downloaded by University of Minnesota - Twin Cities on 20 January 2013

View Article Online

program. In the direct dynamics calculations, MEPs in isoinertial coordinates are calculated using a reorientation of dividing surface (RODS) algorithm.[81]

It should be noted that transition state theory assumes that the internal states of the reactants are in local equilibrium, where the word "local" in this context means[82] that the products need not be present in their equilibrium population. Therefore, for unimolecular reactions in a liquid, transition state theory assumes that the coupling of the solvent to the reacting solute is strong enough to maintain an equilibrium population of reactants,[10,83] and for bimolecular reactions it also assumes that diffusion is fast enough to maintain a local equilibrium concentration of reacting partners in the vicinity of each reactant molecule. For unimolecular reactions in the gas phase, transition state theory yields what is conventionally called the high-pressure limit (in which the pressure is high enough to maintain local equilibrium of reactant states), although it is actually a plateau reached before one enters the suprahigh-pressure regime.[22] For gas-phase bimolecular reactions, the rate constant is only well defined if[84] the time for reaction is much greater then the time for establishment of local equilibrium among the reactant states, which in turn is much higher than the time for passage of a system through the transition state region of phase space; that is, the system must be in the high-pressure limit but not the suprahigh pressure limit. The rate evaluated by transition state theory corresponds to a high enough pressure that energy transfer collisions repopulate the reactive states of the reactants to maintain a thermal distribution, but a more general statement about the pressure regime to which the TST rate constant applies requires a consideration of possible intermediates, and we will defer this discussion to subsection II. D.

It is important to note that the validity of the equilibrium assumption of transition state theory is a function of the more than just the total pressure. Consider again that the basic assumption in transition state theory is that the conformational states of the reactants are in local equilibrium with each other, and this equilibrated pool of states of the reactants and the transition state are in quasiequilibrium during the reaction. When this assumption is applied to MS-VTST and MP-VTST, it means that the interconversion between the conformations of reactant is much faster than the chemical reaction, and one sometimes morphs this into a statement that torsional barriers of reactants are much smaller than the barriers of chemical reaction. However, that is an oversimplification, as seen by considering the reaction of ethanol with hydroxyl radical. The torsional barriers of ethanol are as high as $\sim$3 kcal mol^{-1}, which makes them similar to or even larger than the reaction barriers studied in the present work. But under the experimental conditions where the reaction has been studied, the concentration of hydroxyl radical is much lower than that of ethanol, and it is reasonable to assume that the conformations of ethanol are in quasiequilibrium during the reaction. Therefore MS-VTST and MP-VTST are still applicable for these reactions.

In general we label the reactant conformations by $j = 1, 2,\ldots, J$ and we label the transition state conformations by $k = 1, 2,\ldots, K$, and we note that for a unimolecular reaction, one can rewrite the rate constant of eqn (17) as

$$k^{\text{MP-VTST}} = \frac{\sum_{k=1}^{K} s_k}{R} \tag{29}$$

where

$$R = \sum_{j=1}^{J} r_j \tag{30}$$

$$r_j = Q_{\text{elec}}^{\text{R}} Q_j^{\text{S,R}} \tag{31}$$

Downloaded by University of Minnesota - Twin Cities on 20 January 2013
Published on 29 February 2012 on http://pubs.rsc.org | doi:10.1039/C2FD20012K

 This journal is © The Royal Society of Chemistry 2012

and

$$s_k = \frac{k_B T}{h} Q^{\ddagger}_{elec} \exp\left(-V^{\ddagger}/k_B T\right) \kappa_k \Gamma_k Q^{S,\ddagger}_k \quad (32)$$

Note that the barrier $V^{\ddagger}$ in eqn (32) is the energy difference between the lowest-energy saddle point (*i.e.*, lowest-energy conformation of the transition state) and the lowest-energy conformation of the reactant, and the relative energy of conformation k is included in $Q^{S,\ddagger}_k$ *via* the Boltzmann factor of eqn (5).

It is interesting to compare eqn (29) to the so called generalized Winstein–Holness (GWH) equation,[85–87] which is given by

$$k^{GWH} = \sum_{j=1}^{J} P_j k^{[j]} \quad (33)$$

where we have denoted the equilibrium population of conformer j by

$$P_j = \frac{r_j}{R} \quad (34)$$

and we have associated a rate constant, $k^{[j]}$, with each conformation of reactants. (When there are two conformers of the reactant and two transition-state structures, the GWH equation reduces to the Winstein–Holness (WH) equation.) Eqn (33) can be derived from eqn (29) if we set

$$k^{[j]} = \sum_{k \subset j(k)} \frac{k_B T}{h} \frac{Q^{\ddagger}_{elec}}{r_j} \exp\left(-V^{\ddagger}/k_B T\right) \kappa_k \Gamma_k Q^{S,\ddagger}_k \quad (35)$$

where the sum is over those k that appear in a $j(k)$ for the j on the left hand side, and if we assume that two different conformers of the reactant never lead to the same conformer of the transition state; then we may associate a unique reactant conformer $j(k)$ with each transition state conformer k. (If more than one reactant conformer reacts through the same transition state conformation, then more than one $j(k)$ has the same k.) But this assumption—made to obtain eqn (33)— is not consistent with TST or with the local equilibrium condition of eqn (34). Transition state theory assumes that the rate constants for interconverting conformers of the reactant are larger than the rate constants for chemical reaction—in order to assure local equilibrium. But consider a case where local equilibrium is maintained because the barriers for interconversion of reactant conformers are lower than the barriers to reaction. Since the reaction in such a case is dominated by states with energies higher than the conformational barriers, one cannot associate a given transition state conformer with a unique path originating from a specific reactant conformer. If the barriers between reactant structures are high, they should be considered as two different reactants, not as conformers of a single reactant. Furthermore, eqn (33) is wrong in the general case. Consider, for example, a case with two similar conformations of the reactants and one conformation of the transition state. Then $k^{[2]} \approx k^{[1]}$, and eqn (33) predicts a rate constant equal to $\sim k^{[1]}$, but the correct answer is $\sim k^{[1]}/2$. (Note, as an aside, that the Curtin–Hammett principle does not suffer from this error, although some derivations[88] of it do suffer from it because they are based on the GH equation, which is inconsistent, *i.e.*, wrong.)

However, transition state theory can be formulated to handle multiple conformers properly, and that is what we have done in MS-VTST and MP-VTST. Unlike the GWH equation, we do not assume that one can identify one-to-one connections between transition state conformations and reactant conformations. Furthermore our treatment remains valid even in the regime that torsions are better descried as hindered rotors than as a collection of individual conformational states. The fact that the MS-VTST and MP-VTST methods do not require one to map the routes

Published on 29 February 2012 on http://pubs.rsc.org | doi:10.1039/C2FD20012K
Downloaded by University of Minnesota - Twin Cities on 20 January 2013

View Article Online

between the conformations of the saddle point and the conformations of the reactants or reactants is a key advantage of the correct formulation of transition state theory. The MS-VTST and MP-VTST methods fully account for the very likely reactive events in which the molecular system crosses from one reaction valley to another on the route to the transition state, contrary to the claim[87] that TST cannot handle this or the assumption[88] that this does not occur.

II. D. The treatment of intermediates

Consider a bimolecular gas-phase reaction of A with B, with a pre-reactive intermediate:

$$A + B \rightarrow AB \rightarrow AB^{\ddagger} \rightarrow P \tag{36}$$

where AB is an intermediate complex, $AB^{\ddagger}$ is the transition state, and P is the product. The reaction rate may be written as

$$\frac{d[P]}{dt} = k_{bimol}[A][B] \tag{37}$$

where, as usual, brackets denote concentrations. If the reactants A and B are in quasiequilibrium with the transition state (where quasiequilibrium is the same as equilibrium except that products and transition state species arising from products are missing), then it may be reasonable to assume that they are also in local equilibrium with AB. In that case, we can also write

$$\frac{d[P]}{dt} = k_{unimol}[AB] \tag{38}$$

where

$$k_{unimol} = k_{bimol}/K \tag{39}$$

and K is the equilibrium constant for $A + B \rightarrow AB$. Because TST assumes local equilibrium on the reactant side of the transition state, the reaction rates computed by TST are consistent with eqn (39). Because of eqn (39), the VTST rate constant with $\kappa = 1$ is independent of whether we use eqn (38) or (37). (A related but somewhat different issue is whether the canonical treatment is adequate. We note that in the case that $\tilde{U}^{VTS}$ is below the reactant ZPE (or in fact whenever it is below V_a^{AG}), the improved canonical variational transition state theory[75,89–91] (ICVT) can be used to exclude the contribution of the states with total energies lower than the V_a^{AG} in the partition function.) However, when we incorporate tunneling, the ground-state tunneling approximation depends on whether or not we assume that the complex is equilibrated, so further considerations are needed, as discussed next.

TST has the requirement that the pressure must be high enough to establish local equilibrium among the states of A and the states of B even if the concentration of AB is not at local equilibrium. Notice that local equilibrium among the states of A and the states of B is easily achieved in the presence of an inert gas. Inert gas collisions can equilibrate A and B by bimolecular collisions, but thermalization of AB complexes requires termolecular collisions involving at least one A and at least one B.

Notice that the local equilibrium for configurations (such as those corresponding to AB) between A + B and $AB^{\ddagger}$ is generated in two ways. First is by nonreactive collisions with other constituents of the gas. Second, even without collisions with other bodies, is by uninterrupted evolution of the reactant local equilibrium distribution toward the transition state as governed by the Liouville equation.[84] There is, however, an important difference between these two mechanisms. The former populates all states between A + B and $AB^{\ddagger}$. The latter populates only those states that can be reached by conservation of energy and angular momentum. We will

Published on 29 February 2012 on http://pubs.rsc.org | doi:10.1039/C2FD20012K
Downloaded by University of Minnesota - Twin Cities on 20 January 2013

 This journal is © The Royal Society of Chemistry 2012

View Article Online

focus on the energetic criterion. If the complex has states of lower energy than the lowest-energy state of A + B, then those states cannot be populated without termolecular collisions. If termolecular collisions are insufficient to populate the low-energy states of AB, then those states will be missing.

For the reactions studied in this article, all the $\tilde{U}_k^{\mathrm{VTS}}$ are higher than the reactant ZPE. In this article, we consider the low-pressure limit in which the system reaches local equilibrium only by the Liouville equation. Therefore the states with total energies lower than the lowest-energy state of ethanol + OH are not used for tunneling calculations because of the ground-state tunneling approximation (which deserves re-examination in this light, as discussed below). However, if one calculates k_{unimol} followed by setting k_{bimol} equal to Kk_{unimol}, which is the high-pressure limit, then those states will be present in the tunneling calculation, and the calculated tunneling contribution will be larger.

We evaluated the termolecular collision rate k_{termol} by using the method in ref. 92 and the method in ref. 93 and 94. The two methods predict values of k_{termol}, the rate constant for termolecular collision of ethanol, OH, and helium, that differ by two orders of magnitude. If we assume the third body in termolecular collision in ethanol + OH reaction is helium and its partial pressure is 40 torr, our calculated bimolecular rate constant at 298 K is in the middle of the values of k_{termol}[He] evaluated by the two methods. These rough estimates are insufficient to assess the role of pre-reactive collision complexes under the experimental conditions that have been used to study the reaction of ethanol with hydroxyl. A more reliable treatment of the role of the complex AB under experimental conditions and the fall off in rate constant from the high-pressure plateau is to solve the master equation,[22] which is beyond the scope of the present article. Therefore we simply report calculations in the low-pressure limit.

Published on 29 February 2012 on http://pubs.rsc.org | doi:10.1039/C2FD20012K
Downloaded by University of Minnesota - Twin Cities on 20 January 2013

II. E. Dual-Level strategy

The computation of κ_k and Γ_k can be expensive because it requires the calculation of a reaction path and the Hessians required for generalized normal mode analyses along that path. In a direct dynamics calculation, a reaction path is usually calculated with a density functional that gives a barrier height close to the accurate (or best estimate) barrier height. However, the difference, $\delta V_{\mathrm{corr}}^{\ddagger}$, between the barrier height $V_{\mathrm{DFT}}^{\ddagger}$ calculated by this density functional and the best estimated barrier height $V_{\mathrm{BE}}^{\ddagger}$ is usually nonzero. To account for this difference, we multiply the computed MP-VTST and MS-VTST rate constants by $\exp(-\delta V_{\mathrm{corr}}^{\ddagger}/k_{\mathrm{B}}T)$ where

$$\delta V_{\mathrm{corr}}^{\ddagger} = V_{\mathrm{BE}}^{\ddagger} - V_{\mathrm{DFT}}^{\ddagger} \tag{40}$$

This kind of correction should be used only when $\delta V_{\mathrm{corr}}^{\ddagger}$ is quite small (for instance, less than a few tenths of a kcal mol^{-1}). When $\delta V_{\mathrm{corr}}^{\ddagger}$ is larger, although the barrier is corrected, the reaction path used to calculate tunneling and recrossing effects could be quite inaccurate.

III. Results and discussion

III. A. Geometries and energies of saddle points

We calculated barrier heights of saddle points 1 and 2 of reaction R1a using the M08-SO/ma-TZVP and M08-HX/ma-TZVP methods. These methods respectively yield −0.13 and 1.00 kcal mol^{-1} for the barrier of reaction R1a. The former is in good agreement with our best estimate (which is 0.05 kcal mol^{-1}, as shown in Table 1). To check the geometry effect on calculated barrier heights, we calculated the barrier height by the M08-SO/ma-TZVP//M08-HX/6-31+G(d,p) method, which gives a barrier −0.10 kcal mol^{-1}; this value with the double zeta geometry is in good agreement with the value of −0.13 kcal mol^{-1} obtained with the consistently

View Article Online

Table 1 Energies[a] (kcal mol^{-1}) of ethanol and saddle points at geometries optimized by M08-HX/6-31+G(d,p) method

		CCSD(T)		BE		
Species	Structure	TZ[b]	QZ[c]	DZ[d]	maug-DZ[e]	T_1[f]
ethanol + OH	*trans*	0.00	0.00	0.00	0.00	0.010
	g+/g$^-$[g]	0.12	0.11			
R1a saddle point	1, 2	0.21	0.35	0.12	0.05	0.026
	3, 4	0.23	0.39			0.026
R1b saddle point	1, 2	2.16	2.29	2.03	2.02	0.026
	3, 4	2.23	2.38	2.13	2.10	0.025
	5, 6	2.51	2.68			0.025
	7, 8	2.61	2.74			0.026
	9, 10	4.70	4.83			0.026
	11, 12	5.00	5.12			0.025
	13, 14	5.52	5.63			0.026
R1c saddle point	1, 2	3.31	3.60	2.42	2.74	0.042
	3, 4	3.51	3.79			0.046
	5, 6	3.93	4.19			0.039

[a] All relative energies in this article include a spin–orbit energy −0.20 kcal mol^{-1} for OH radical, and all energies in this table are zero-point exclusive. [b] The CCSD(T)-F12a/aug-cc-pVTZ method. [c] The CCSD(T)-F12b/may-cc-pVQZ method. [d] The cc-pVDZ basis set is used in eqn (2). [e] The maug-cc-pVQZ basis set is used in eqn (2). [f] Calculated by UCCSD/may-cc-pVQZ method. [g] These are the two *gauche* structures.

optimized triple zeta geometry optimization mentioned above. Therefore we conclude, as expected, that no significant error is incurred by using the geometries optimized by the smaller basis set. We therefore performed the rest of the geometry optimizations and all the reaction-path calcuations with the smaller basis set.

We performed an exhaustive conformational structure search for the saddle points of the three reactions by generating guessed conformations based on a set of grids of torsional angles, and we optimized these conformational structures using the M08-HX/6-31+G(d,p) method. Four distinguishable structures (2 pairs of mirror images) were found for the transition state of reaction R1a. Reaction R1b has 14 saddle points (seven pairs of mirror images), and reaction R1c has six saddle points (three pairs of mirror images). Ethanol has three conformational structures. The structures of the saddle points are shown in Fig. 2–4. Previous theoretical studies[40,42,43] only considered one saddle point for each reaction in their calculations, and torsions were modeled by a one-dimensional approximation[40,43] or approximated as harmonic oscillators.[42] Because the Cartesian coordinates are not available in previous reports,[40,42,43] we do not compare our optimized geometries with previous work, and the comparison of our calculated barrier heights with other previous work leaves some questions unanswered, especially for R1b since it has several saddle points with similar energies and conformations.

Single-point energies of all the conformational structures (ethanol, hydroxyl radical, and saddle points) optimized by the M08-HX/6-31+G(d,p) method were calculated by CCSD(T)-F12a/aug-cc-pVTZ and CCSD(T)-F12b/may-cc-pVQZ, respectively. The total energy of the all-*trans* structure of ethanol infinitely separated from hydroxyl radical is taken as the zero of energy, and the relative energies of all the conformational structures are given in Table 1. The relative energies include a −0.20 kcal mol^{-1} spin-orbit energy for the hydroxyl radical. We corrected the barrier heights calculated by the CCSD(T)-F12b/may-cc-pVQZ method using eqn (1) and (2). By applying two basis sets, cc-pVDZ and maug-cc-pVDZ, in the FBS corrections, we checked the convergence of the high-level correction with respect to adding diffuse basis functions.

Published on 29 February 2012 on http://pubs.rsc.org | doi:10.1039/C2FD20012K
Downloaded by University of Minnesota - Twin Cities on 20 January 2013

 This journal is © The Royal Society of Chemistry 2012

View Article Online

Published on 29 February 2012 on http://pubs.rsc.org | doi:10.1039/C2FD20012K
Downloaded by University of Minnesota - Twin Cities on 20 January 2013

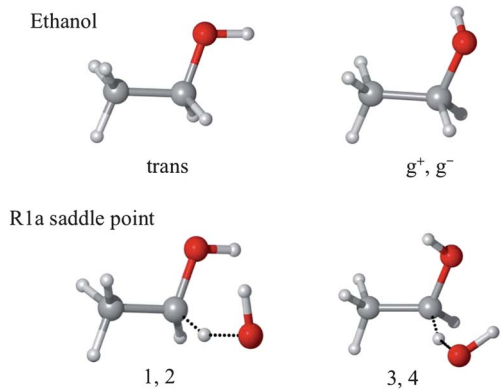

Fig. 2 Conformations of ethanol and saddle points of reaction R1a. Only one structure of each pair of mirror images is shown.

In Table 1, the CCSD(T)-F12b/may-cc-pVQZ energies are considered to be the highest quality CCSD(T)/CBS method, and they are used as the CBS result in eqn (1). As shown in Table 1, for R1a and R1b the energy differences between saddle points calculated by aug-cc-pVTZ and may-cc-pVQZ are under 0.2 kcal mol^{-1}, whereas those for R1c saddle point energies are under 0.3 kcal mol^{-1}, and the differences for reactants are 0.01 kcal mol^{-1}. We only performed the $CCSDT(2)_Q$ calculations for a few low-energy conformations of ethanol and the saddle points due to the very large computational cost. The high-level FBS correction (eqn (2)) with the larger (maug-cc-pVDZ) basis set lowers the CCSD(T) barrier heights of the three reactions by ~0.3 kcal mol^{-1} for R1a and R1b and by 0.9 kcal mol^{-1} for R1c. Furthermore, for R1c the two high-level FBS corrections differ by 0.3 kcal mol^{-1}, which indicates that a larger basis set needs to be used in eqn (2) which is not affordable with our available computational resources. The large size of the $CCSDT(2)_Q$ correction and the large T_1 diagnostic values (see Table 1) indicate that the R1c saddle points have significant multi-reference character. Our values for T_1 for the saddle points of R1c are consistent with the value of 0.044 reported by Galano *et al.*[95] with a different basis set.

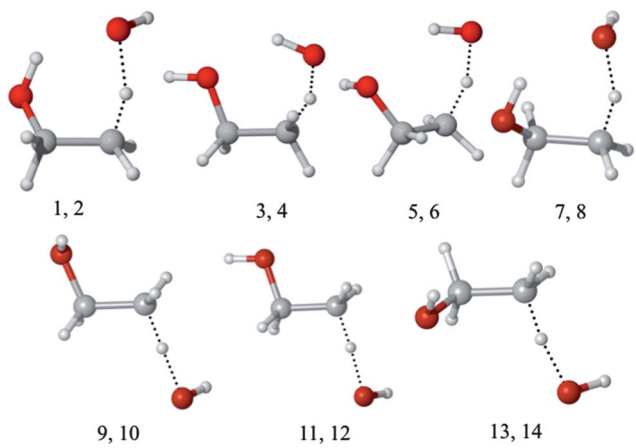

Fig. 3 Saddle points of reaction R1b. Only one structure of each pair of mirror images is shown.

View Article Online

Downloaded by University of Minnesota - Twin Cities on 20 January 2013
Published on 29 February 2012 on http://pubs.rsc.org | doi:10.1039/C2FD20012K

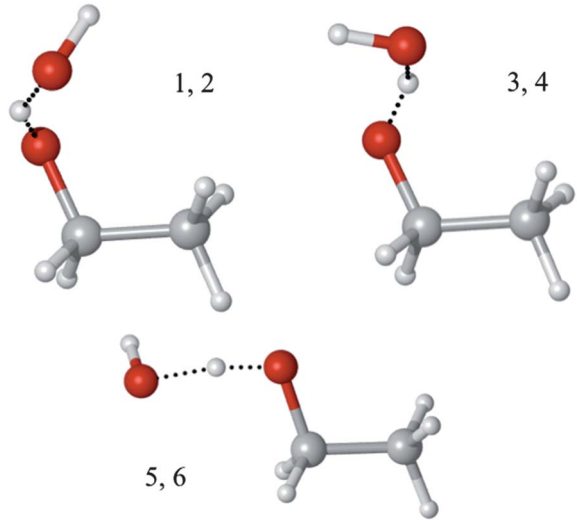

Fig. 4 Saddle points of reaction R1c. Only one structure of each pair of mirror images is shown.

According to the figures in the papers, the studies by Galano *et al.*[42] and Xu *et al.*[43] both used saddle point 1 or 2 (shown in Fig. 2.) for reaction R1a and used saddle point 5 or 6 (shown in Fig. 4) for reaction R1c. Saddle point 1 or 2 of reaction R1a is the lowest-energy saddle point of that reaction according to the CCSD(T)-F12b/may-cc-pVQZ method. However, saddle point 5 or 6 of reaction R1c is the highest-energy conformation, and it is higher than the lowest-energy saddle point of R1c by 0.6 kcal mol^{-1}. The saddle points of reaction R1b can be categorized into two groups, *i.e.*, hydrogen-bonded structures (structures 1–8 in Fig. 3) and non-hydrogen-bonded structures (structures 9–14 in Fig. 3). The structures in each group are similar in energy. In general, the non-hydrogen-bonded structures are higher than the hydrogen-bonded structures by 2–3 kcal mol^{-1}. The structures

Table 2 Calculated zero-point exclusive barrier heights[a] (kcal mol^{-1}) with various density functionals using the 6-31+G(d,p) basis set

Saddle point	M08-HX	M08-SO	M06-2X	M05-2X
R1a (1, 2)	0.17	−0.87	−0.51	−0.13
R1b (3, 4)	0.31	−0.81	−0.47	−0.18
R1b (1, 2)	1.86	0.24	1.03	1.32
R1b (3, 4)	1.57	0.26	0.85	1.13
R1b (5, 6)	2.03	0.67	1.22	1.44
R1b (7, 8)	2.37	0.80	1.56	1.88
R1b (9, 10)	5.42	4.05	4.51	4.63
R1b (11, 12)	5.55	4.15	4.68	4.86
R1b(13, 14)	6.24	4.95	5.37	5.64
R1c (1, 2)	2.55	0.69	0.55	1.24
R1c (3, 4)	2.66	0.85	0.70	1.39
R1c (5, 6)	3.47	1.45	1.27	1.85

[a] The energy of *trans*-ethanol plus hydroxyl radical is taken as zero of energy.

 This journal is © The Royal Society of Chemistry 2012

View Article Online

for R1b used in the works by Galano *et al.*[42] and Xu *et al.*[43] are one of the hydrogen-bonded structures according to the hydroxyl group orientation shown in their figures. The structures of the saddle points used in the work by Sivaramakrishnan *et al.*[40] are not clear since neither figures nor coordinates are provided in the paper. However they[40] do remark about R1b saddle points that "Our calculations find that the H-bonded saddle point lies 1.4 kcal mol^{-1} higher in energy than the geometry of Xu and Lin and also has significantly less entropy." This remark is contradictory to our findings and also is contradictory with the common expectation that an H bond usually lowers conformational energy. Even if the previous studies used the lowest-energy saddle point, they would still incur error from using only one structure[42] or from including other structures only by uncoupled one-dimensional treatments of torsions.[40,43]

Table 2 lists the calculated energies of the saddle points with various density functionals using the 6-31+G(d,p) basis set. The purpose of using such a small basis set with density functional theory is to find an efficient and affordable method for direct

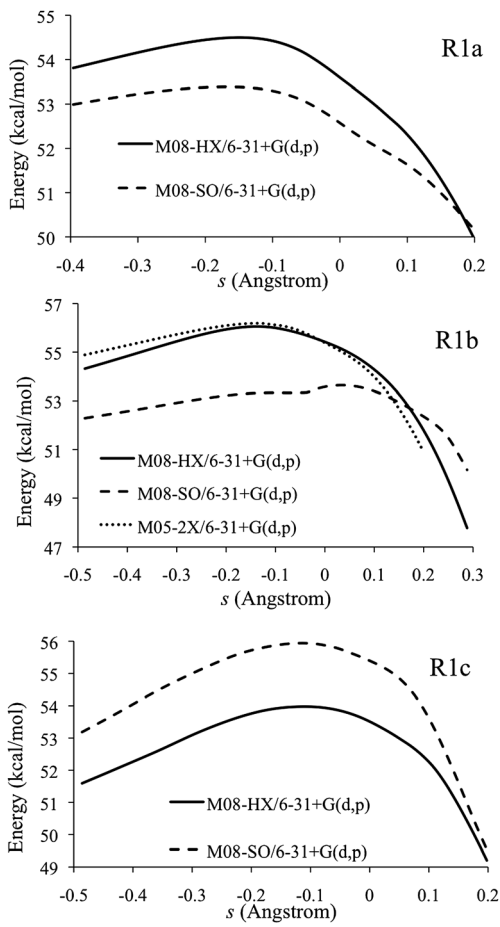

Fig. 5 The lowest-energy vibrationally adiabatic ground-state potential energy $\tilde{U}_1$ curves for each of reactions R1a–R1c. The $\tilde{U}_1$ curves of reaction R1b are calculated by using density functional integration grids that have 96 radial shells around each atom and a spherical product angular grid having 32 θ points and 64 φ points in each shell in the integrations. The $\tilde{U}_1$ curves of R1a and R1c are calculated by using density functional integration grids that are pruned from grids having 99 radial shells around each atom and 974 angular points in each shell.

Downloaded by University of Minnesota - Twin Cities on 20 January 2013
Published on 29 February 2012 on http://pubs.rsc.org | doi:10.1039/C2FD20012K

View Article Online

Downloaded by University of Minnesota - Twin Cities on 20 January 2013
Published on 29 February 2012 on http://pubs.rsc.org | doi:10.1039/C2FD20012K

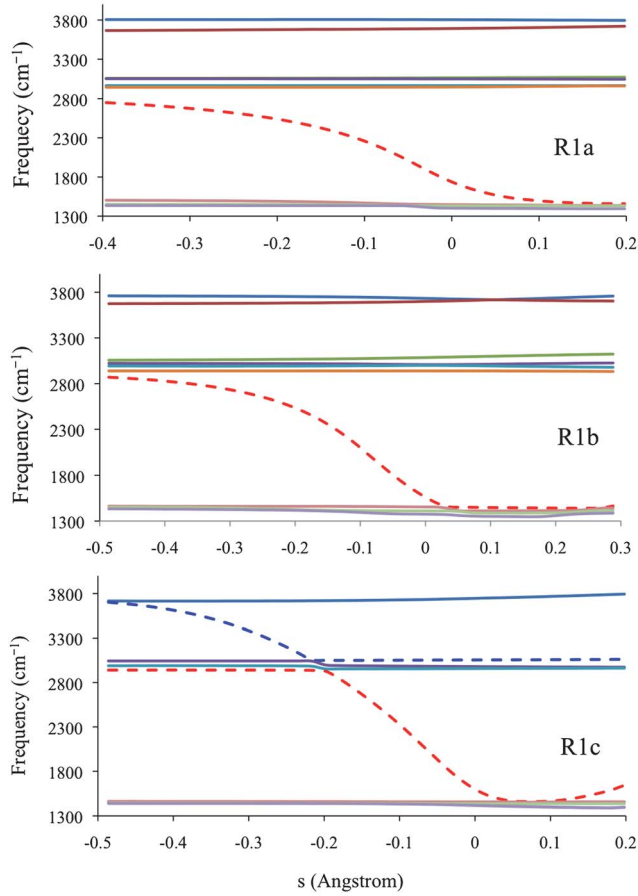

Fig. 6 The highest ten frequencies along the reaction paths of R1a–R1c calculated by the M08-HX/6-31+G(d,p) method. The frequencies are scaled by a factor of 0.972 by scaling all Hessian elements as explained in the text. These paths are the lowest-energy paths of each reaction. For the R1c reaction, two frequencies that remain almost constant between 2800 cm^{-1} and 3300 cm^{-1} are removed for better visualization.

dynamics calculations. The barrier heights by the M08-HX/6-31+G(d,p) method are in agreement with the best estimates of barriers within 0.2 kcal mol^{-1}. Therefore the M08-HX/6-31+G(d,p) method is used for straight direct dynamics calculations except where specified otherwise.

III. B. Generalized normal modes

In order to calculate variational effects, we need to calculate $G_{T,k}$ as a function of s, and in order to calculate tunneling probabilities we need to calculate $\tilde{U}_k$ as a function of s. These are calculated in the quasiharmonic approximation from generalized normal mode frequencies calculated in curvilinear coordinates[17,96] (which means that the facets of Fig. 1 are actually curved).

In our generalized normal mode analyses, a set of non-redundant internal coordinates is used, in particular, 10 bond stretches, 13 bond angles, and 4 dihedral angles (each dihedral angle corresponds to a torsion mode).

One interesting question is how many torsions there are in the saddle points of R1a–R1c. In this work, four internal rotations, namely those around the C1–O and C1–C2

 This journal is © The Royal Society of Chemistry 2012

View Article Online

Table 3 Torsional anharmonicity factors[a] of ethanol and three transition states

T/K	$F^{MS,E}$	$F^{T,E}$	$F^{MS\text{-}T,E}$	$F^{MS,R1}$	$F^{T,R1}$	$F^{MS\text{-}T,R1}$	$F^{MS,R2}$	$F^{T,R2}$	$F^{MS\text{-}T,R2}$	$F^{MS,R3}$	$F^{T,R3}$	$F^{MS\text{-}T,R3}$
200	2.6	1.2	3.1	4.4	1.1	4.8	6.7	1.1	7.4	4.4	1.2	5.1
250	2.7	1.2	3.3	4.4	1.1	4.9	7.4	1.1	8.4	4.9	1.2	5.9
298	2.7	1.2	3.4	4.4	1.1	5.0	8.4	1.2	9.8	5.3	1.2	6.6
300	2.7	1.2	3.4	4.4	1.1	5.0	8.5	1.2	9.9	5.3	1.2	6.6
400	2.8	1.3	3.6	4.4	1.2	5.3	11.9	1.2	13.9	5.9	1.3	7.8
500	2.9	1.3	3.7	4.4	1.3	5.7	16.4	1.1	18.2	6.3	1.4	8.7
600	2.9	1.3	3.7	4.4	1.3	6.0	21.3	1.0	22.2	6.7	1.4	9.4
700	2.9	1.3	3.7	4.5	1.4	6.2	26.4	1.0	25.6	6.9	1.4	10.0
800	2.9	1.2	3.6	4.5	1.5	6.5	31.5	0.9	28.3	7.1	1.5	10.4
900	3.0	1.2	3.6	4.5	1.5	6.7	36.4	0.8	30.4	7.3	1.5	10.7
1000	3.0	1.2	3.5	4.5	1.5	6.9	41.0	0.8	31.9	7.4	1.5	10.9
1500	3.0	1.0	3.0	4.5	1.7	7.4	60.3	0.6	34.0	7.9	1.4	10.8
1800	3.0	0.9	2.8	4.5	1.7	7.5	69.0	0.5	32.8	8.1	1.3	10.3
2000	3.0	0.9	2.7	4.5	1.6	7.4	74.0	0.4	31.7	8.1	1.2	9.9
2400	3.0	0.8	2.4	4.5	1.6	7.1	82.2	0.4	29.0	8.3	1.1	9.0

[a] Geometries and Hessians are calculated by the M08-HX/6-31+G(d,p) method and energies are calculated by the CCSD(T)-F12b/may-cc-pVQZ method.

Table 4 Reaction torsional anharmonicity factors calculated by eqn (10)

T/K	R1a	R1b	R1c
200	1.6	2.4	1.7
250	1.5	2.6	1.8
298	1.5	2.9	1.9
300	1.5	2.9	1.9
400	1.5	3.9	2.2
500	1.5	5.0	2.4
600	1.6	6.0	2.6
700	1.7	7.0	2.7
800	1.8	7.8	2.9
900	1.9	8.6	3.0
1000	2.0	9.2	3.1
1500	2.4	11.1	3.5
1800	2.7	11.7	3.7
2000	2.8	11.9	3.7
2400	3.0	12.1	3.8

bonds of ethanol and those around the C···H (or O···H in R1c) and O···H partial bonds, are treated with torsional anharmonicity. The bond angle between the two partial bonds involving the transferring H atom is not linear; the C···H···O bond angles of saddle points of R1a and R1b are in the range of 152 deg to 172 deg, and the O···H···O bond angles of saddle points of R1c are 144° and 145°. A linear bend would correspond to two degenerate or nearly degenerate vibrational modes and one less torsion, but no such degenerate or nearly degenerate modes are observed in the normal mode analyses. For example, the C···H···O bending motion in the structure in which this angle is 172 deg is mostly distributed over two normal modes, in each of which it is mixed with other motions, and these modes have frequencies of 1161 and 984 cm^{-1}.

The three reactions considered here, especially R1a, have quite low barriers so that the potential energy curves in the vicinity of saddle points change quite slowly, and the locations of the maxima of the vibrationally adiabatic ground state potential

Downloaded by University of Minnesota - Twin Cities on 20 January 2013
Published on 29 February 2012 on http://pubs.rsc.org | doi:10.1039/C2FD20012K

View Article Online

curves or of the low-temperature generalized free energy of activation profiles depend sensitively on converging the frequency calculations. Therefore, to calculate a converged vibrationally adiabatic ground-state potential energy curve, it is essential to use a sufficiently fine grid for integration in the density functional calculations. The vibrationally adiabatic ground-state potential curves for the lowest-energy saddle points ($k = 1$) of the three reactions are shown in Fig. 5, as calculated with the grids specified in subsection II. A. These curves show that the maxima are located at a significant distance away from the conventional transition state ($s = 0$) in all three reactions. For example, the maximum of the $\tilde{U}_1$ curve for R1a is at $s = -0.14$ Å and is higher than the conventional transition state by 0.9 kcal mol^{-1}. The variational transition states of R1a are located between -0.18 Å and -0.15 Å for the temperatures 200–2400 K. Fig. 6 shows the ten largest frequencies calculated by the M08-HX/6-31+G(d,p) method along the lowest-energy reaction paths of reaction R1a–R1c. One frequency (dashed line in red in Fig. 6) changes dramatically in the vicinity of saddle point, in particular, this frequency decreases by 800 cm^{-1} from $s = -0.2$ Å to $s = 0$. This frequency is the vibration of the breaking bond that is turning into the vibration of the making bond.

III. C. Torsional anharmonicity

The MS-T method is applied to ethanol and the transition states of the three reactions to account the torsional anharmonicity. In the MS-T calculations, the geometries and Hessians are calculated by the M08-HX/6-31+G(d,p) method and energies are calculated by the CCSD(T)-F12b/may-cc-pVQZ method. Table 3 lists torsional anharmonicity factors calculated by eqn (6), (8), and (9) for ethanol and the three transition states. Table 4 lists the reaction torsional anharmonicity factors calculated by eqn (10) for the three reactions.

The torsional anharmonicity factors $F^{\mathrm{MS-T}}$ for rate calculations are based on M08-HX/6-31+G(d,p) geometries and Hessians even though κ_k and Γ_k are calculated by using other potential energy surfaces in some cases. Note that Hessians obtained by these two methods are scaled by their scaling factors that were optimized[36] for obtaining accurate zero-point energy. We compared the $F^{\mathrm{MS-T}}$ factors obtained by using the CCSD(T)-F12a/may-cc-pVQZ//M08-HX/6-31+G(d,p) to those obtained by using the CCSD(T)-F12a/may-cc-pVQZ//M05-2X/6-31+G(d,p) potential energy surfaces and found that they differ by less than or equal to 12%, which is similar to or smaller than the uncertainties of the dynamics methods. Therefore we conclude that it is an acceptable approximation to use slightly different potential energy surfaces for anharmonicity and for dynamics calculations.

In our previous study,[64] we calculated partition functions of ethanol by using the one-dimensional (1-D) torsional eigenvalue summation (TES) method for its torsional modes. In ethanol, the two internal rotations are nearly separable in internal coordinates (note that the normal modes of the two torsions are mixtures of the two torsions), therefore the 1-D TES method in internal coordinates is applicable to ethanol. The partition functions calculated by the MS-T method in this work and the TES method used in previous work[30] differ by about 22% at 200 K, 7% at 1000 K, and 3% at 2000 K. These differences are acceptable for treatment of the torsions.

The internal rotations of the saddle points are strongly coupled together except for the methyl group rotation of the R1a and R1c saddle points. The local periodicities of the strongly coupled torsions are calculated by Voronoi tessellation.[64,65] Fig. 7 shows a contour plot of the two-dimensional torsional potential energy surface of the R1a transition state. The two dimensions are the H–O–C1–C2 dihedral angle and H–O–H–C1 dihedral angle. Potential energies are calculated by the M08-HX/6-31+G(d,p) method. The other geometrical parameters are fixed at saddle point 1 of this reaction. There are two minima on the potential energy surface. Note that C1 is a chiral center, and the mirror images of these two minima cannot be generated

Published on 29 February 2012 on http://pubs.rsc.org | doi:10.1039/C2FD20012K
Downloaded by University of Minnesota - Twin Cities on 20 January 2013

 This journal is © The Royal Society of Chemistry 2012

View Article Online

Downloaded by University of Minnesota - Twin Cities on 20 January 2013
Published on 29 February 2012 on http://pubs.rsc.org | doi:10.1039/C2FD20012K

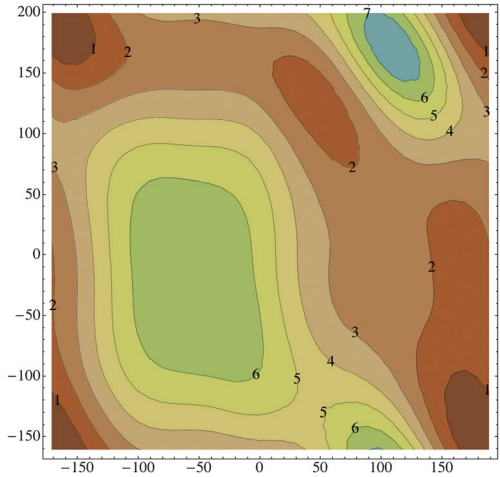

Fig. 7 Two-dimensional contour plot of the torsional potential energy surface of the R1a transition state. The abscissa is the H–O–C1–C2 dihedral angle (in degrees) and the ordinate is the H–O–H–C1 dihedral angle (in degrees). The potential energy (in kcal mol^{-1}) is calculated by the M08-HX/6-31+G(d,p) method. The other geometrical parameters are fixed at their values for saddle point 1.

by internal rotations. Fig. 7 shows that two separate 1-D rigid scans cannot yield the correct number of minima. Even if a relaxed scan can follow the minimum-energy path between the two minima, two relaxed scans will give the same information, and the partition function will be overestimated. Therefore the transition state of R1a gives a clear example of the inapplicability of a one-dimensional separable approximation. Nevertheless this approximation is widely used in the literature and has also been used for this reaction.[40]

If we let LH-SS-CVT denote the single-structure results in the quasiharmonic approximation, then the factors in Table 4 give the ratio of MS-CVT to LH-SS-CVT, and they also give the ratio of MS-CVT/SCT to LH-SS-CVT/SCT. These ratios range from 1.5 to more than an order of magnitude (12.1) with a median value of 2.7. Furthermore the factor is significantly different for each reaction and therefore has an important effect on product ratios. Thus multi-structural torsional anharmonicity is a significant factor that should not be neglected even for this small-molecule reaction.

III. D. MS-VTST reaction rate

The rate constants for the three reactions are calculated by using M08-HX/6-31+G(d,p) and M08-SO/6-31+G(d,p) potential energy surfaces, respectively. The calculated total rate constants of the three reactions are plotted in Fig. 8 together with experimental data. We also calculated the branching fraction of the three reactions and plotted them in Fig. 9. The calculated rate constants are fitted to a physically motivated four-parameter expression. This expression and its corresponding activation energy are

$$k = A\left(\frac{T+T_0}{300}\right)^n \exp\left(-\frac{E(T+T_0)}{R\left(T^2+T_0^2\right)}\right) \tag{41}$$

$$E_a = E\frac{T^4+2T_0T^3-T_0^2T^2}{\left(T^2+T_0^2\right)^2}+nR\frac{T^2}{T+T_0} \tag{42}$$

View Article Online

Downloaded by University of Minnesota - Twin Cities on 20 January 2013
Published on 29 February 2012 on http://pubs.rsc.org | doi:10.1039/C2FD20012K

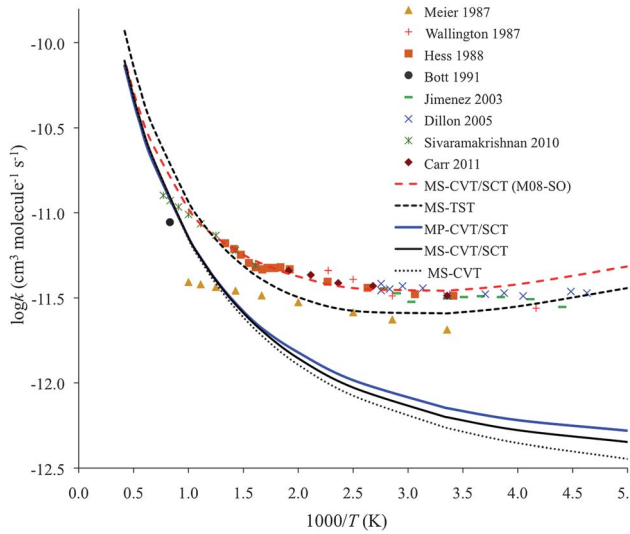

Fig. 8 Total reaction rates of R1a–R1c. The rate constants shown as black or blue solid, dotted, and dashed lines are calculated using M08-HX/6-31+G(d,p) potential energy surfaces. The rate constants shown as a red dashed line are calculated using M08-SO/6-31+G(d,p) potential energy surfaces.

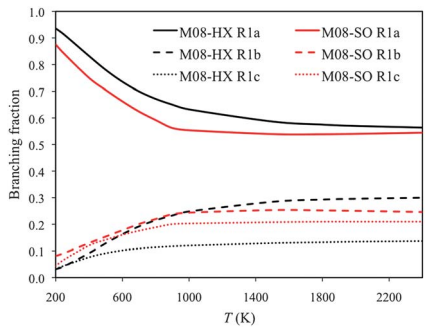

Fig. 9 Calculated branching fractions by M08-HX/6-31+G(d,p) (in black) and M08-SO/6-31+G(d,p) (in red) methods.

where A, n, E, and T_0 are fitting parameters. Eqn (41) is very similar to the eqn (8) in our previous work,[97] but it is more physically meaningful for an exoergic or ergoneutral reaction because it leads to a finite rate constant when T approaches 0 K, as it should in those cases.[98] Furthermore the activation energy becomes 0 at $T = 0$ K. The rate constants obtained by using the M08-HX/6-31+G(d,p) potential energy surfaces are

$$k_{1a} = 7.033 \times 10^{-14} \left(\frac{T + 664.9}{300}\right)^{2.931} \exp\left[-\frac{1.470(T + 664.9)}{R(T^2 + 4.421 \times 10^5)}\right] \quad (43)$$

$$k_{1b} = 9.273 \times 10^{-14} \left(\frac{T + 299.5}{300}\right)^{2.702} \exp\left[-\frac{1.682(T + 299.5)}{R(T^2 + 8.969 \times 10^4)}\right] \quad (44)$$

 This journal is © The Royal Society of Chemistry 2012

View Article Online

$$k_{1c} = 1.278 \times 10^{-14}\left(\frac{T+205.5}{300}\right)^{3.160}\exp\left[-\frac{0.3278(T+205.5)}{R(T^2+4.224\times10^4)}\right] \quad (45)$$

All rate constants are in units of cm^3 $molecule^{-1}$ s^{-1}. The rate constants calculated by using the M08-SO/6-31+G(d,p) potential energy surfaces are

$$k_{1a} = 3.996 \times 10^{-10}\left(\frac{T+1035}{300}\right)^{-0.07942}\exp\left[-\frac{8.209(T+1035)}{R(T^2+1.072\times10^6)}\right] \quad (46)$$

$$k_{1b} = 2.910 \times 10^{-12}\left(\frac{T+650.3}{300}\right)^{1.185}\exp\left[-\frac{3.632(T+650.3)}{R(T^2+4.228\times10^5)}\right] \quad (47)$$

$$k_{1c} = 1.576 \times 10^{-14}\left(\frac{T+575.4}{300}\right)^{3.075}\exp\left[-\frac{0.3118(T+575.4)}{R(T^2+3.311\times10^5)}\right] \quad (48)$$

The M08-HX/6-31+G(d,p) potential energy surfaces are chosen for rate calculations because—among the small-basis-set calculations—they give barrier heights closest to our best estimates (see Tables 1 and 2). The MS-TST rate constants shown in Fig. 6 agree very well with the experimental data. The MS-TST rate constants include the multi-structural torsional anharmonicity, but they locate the reaction bottlenecks at the conventional transition states that are often not the true dynamical bottlenecks along the minimum energy paths, and also they do not include the tunneling contributions. The MS-CVT/SCT rate constants are much lower than the MS-TST rate constants, and they are very close to the MS-CVT rate constants. Therefore the difference between the MS-CVT/SCT and MS-TST rate constants is mainly caused by the variational effect. The combination of a dramatic increase of one frequency and slow changes of potential energies in the vicinity of saddle point causes significant variational effects, *e.g.*, for reaction R1a, CVT rates are lower than TST rates by a factor 10, 5, and 2 at $T = 200$, 300, and 2400 K, respectively. The rate constants calculated by the M08-SO/6-31+G(d,p) potential energy surface have some uncertainties due to the sensitivity of the frequencies to grids, as discussed in Section III B. Using a sufficiently large grid in density functional frequency calculations is especially important for large systems because some small uncertainty in each vibrational frequency can lead to large accumulated errors in large systems that involve a large number of vibrational modes.

Tunneling contributions are not large for these hydrogen-transfer reactions because they all have quite low barrier heights, especially for reaction R1a. Note that the zero-point inclusive barrier of reaction R1a at the conventional transition state (saddle point) is lower than the reactant zero-point inclusive energy. If only the ground-state reaction and the low-pressure plateau (see subsection II. D) were considered, there would be no tunneling because it is reasonable to assume that reactants are not stabilized to a weakly bound reactant complex well at low or medium pressure (*e.g.*, a few hundred torr[35,39] or lower[40] for most experiments that have been conducted). However, the variational transition states of reaction R1a are higher in energy than the reactant by about 0.5 kcal mol^{-1}; therefore a small amount of tunneling is obtained by the SCT method, *e.g.*, tunneling transmission coefficients are 1.2 at 200 K and 1.1 at 300 K, respectively. We note that if the reactant complex were equilibrated with reactants, the energy levels that are below the zero-point energy of the reactants would also need to be considered in the tunneling calculations, which would lead to larger tunneling contributions. This is a good place to

Published on 29 February 2012 on http://pubs.rsc.org | doi:10.1039/C2FD20012K
Downloaded by University of Minnesota - Twin Cities on 20 January 2013

View Article Online

insert a caution about the ground-state tunneling approximation that has usually been used for the transmission coefficient in past work and that is also used here. The ground-state tunneling approximation assumes that the ground-state transmission coefficient is typical of all the transmission coefficients that make a significant contribution to the reaction rate at temperatures low enough for tunneling to be significant.[15,90] However, for a case like the present one, this cuts off tunneling due to the energetic threshold more severely than would be the case for higher-energy states, and so actually one of those higher-energy states might be more typical. This would not make a significant difference for reactions with high barriers, but it is less valid for reactions with low barriers (small positive barrier or negative barrier), such as the present one, for which using a higher-energy state to compute a representative transmission coefficient would increase the calculated rate constant a little at low temperature. We calculated the tunneling with the low energies present and found that the MS-CVT/SCT rate constant for R1a would be increased by factors of 1.8 and 1.2 at 298 and 500 K, respectively.

The MS-CVT/SCT rate constants by the M08-HX/6-31+G(d,p) method are much lower than the experimental ones, although the barrier heights calculated by the M08-HX/6-31+G(d,p) method agree very well with our best estimated values, and important effects are taken into account in the dynamics calculations, in particular, multi-structural torsional anharmonicity, the variational effect, and multi-dimensional tunneling. What could cause this discrepancy between theory and experiment? One possible cause is that our best estimates of barrier heights by coupled cluster theory may be too high. Coupled cluster theory at the CCSD(T) level is usually considered to have chemical accuracy, better than 1 kcal mol^{-1}. In the present case, the FBS correction using the $CCSDT(2)_Q$ method lowers the barrier heights calculated by the CCSD(T) method, but the best estimates of the barriers may be still higher than the accurate ones. Therefore we performed rate calculations using the M08-SO/6-31+G(d,p) method, which gives 1 kcal mol^{-1} lower barrier than the M08-HX/6-31+G(d,p) method. As shown in Fig. 8, the rate constants obtained by the M08-SO/6-31+G(d,p) method agree with experimental data very well. We conclude that the true barrier heights are between the values calculated by the M08-HX/6-31+G(d,p) and M08-SO/6-31+G(d,p) methods.

Some other reasons for the discrepancy between theory and experiment could be the presence of some stabilized pre-reaction complexes or imperfection of the dynamics and the statistical methods. For example, vibrational modes except torsional modes are still treated using a quasiharmonic approximation (harmonic oscillator formulas with frequencies scaled to account for anharmonicity), torsional barrier heights are obtained from local periodicities rather than calculated directly, mode–mode coupling is not fully taken into account for nontorsional modes, and tunneling contributions could be underestimated or overestimated by the SCT method. Furthermore we assume that the torsional anharmonicity factor remains the same at the variational transition state as at the conventional transition state. The last-named issue is particularly troublesome in the present cases because we observe a large variational effect for these reactions that is sensitive to the convergence of the frequencies, but the reaction-path independence of the torsional anharmonicity factor has not been tested.

III. E. MP-VTST reaction rate

In the MP-VTST calculation of each reaction, the M08-HX/6-31+G(d,p) potential energy surfaces are used and the recrossing and tunneling transmission coefficients of all reaction paths are calculated explicitly. For comparison purposes, we also calculate an averaged generalized transmission coefficient $\langle\gamma\rangle_P$ using eqn (25) by considering some low-energy reaction paths for R1b. The calculated MP-CVT/SCT rate constants for the three reactions respectively are

Published on 29 February 2012 on http://pubs.rsc.org | doi:10.1039/C2FD20012K
Downloaded by University of Minnesota - Twin Cities on 20 January 2013

 This journal is © The Royal Society of Chemistry 2012

View Article Online

$$k_{1a} = 8.265 \times 10^{-14}\left(\frac{T+663.9}{300}\right)^{2.869}\exp\left(-\frac{1.396(T+663.9)}{(T^2+4.407\times10^5)}\right) \quad (49)$$

$$k_{1b} = 6.979 \times 10^{-14}\left(\frac{T+327.6}{300}\right)^{2.694}\exp\left(-\frac{1.890(T+327.6)}{(T^2+1.073\times10^5)}\right) \quad (50)$$

$$k_{1c} = 1.285 \times 10^{-14}\left(\frac{T+292.6}{300}\right)^{3.123}\exp\left(-\frac{0.6030(T+292.6)}{(T^2+8.562\times10^4)}\right) \quad (51)$$

The total MP-CVT/SCT rate constants of the three reactions are also plotted in Fig. 8. The difference between MP-CVT/SCT rates and MS-CVT/SCT rates are not noticeable at high temperatures, and they are about 15% at $T = 200$ K.

Fig. 10 shows the recrossing transmission coefficients Γ_k, tunneling transmission coefficients κ_k, and generalized transmission coefficients γ_k or $\langle\gamma\rangle$ as calculated by the M08-HX/6-31+G(d,p) method.

Reaction R1a has two pairs of saddle points that are close in energy with each other. We find that $\langle\gamma\rangle$ and γ_1 are very similar, and therefore a single reaction path can represent the whole reaction very well for this reaction.

The saddle points are more diverse in energy and in geometry for reaction R1b than for R1a and R1c. The corresponding reaction paths have quite different transmission coefficients as shown in Fig. 10. We calculated the generalized transmission coefficient γ_1 (corresponding to the reaction path corresponding the lowest-energy saddle point), $\langle\gamma\rangle_8$ (averaged over the eight reaction paths corresponding the eight

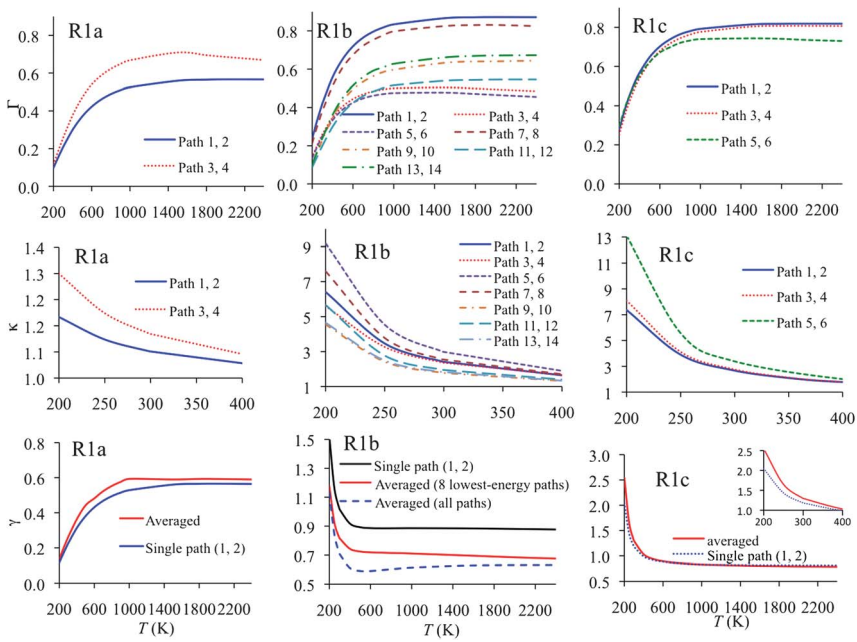

Fig. 10 Recrossing transmission coefficient Γ_k, tunneling transmission coefficient κ_k, and generalized transmission coefficient γ_k or $\langle\gamma\rangle$ of each reaction that are calculated by the M08-HX/6-31+G(d,p) method.

Published on 29 February 2012 on http://pubs.rsc.org | doi:10.1039/C2FD20012K
Downloaded by University of Minnesota - Twin Cities on 20 January 2013

View Article Online

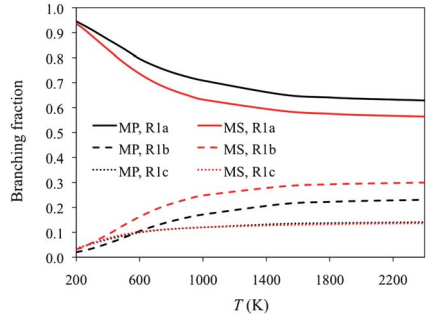

Fig. 11 Calculated branching fractions by the MP-VTST method (in black) and the MS-VTST method (in red). In the MP-VTST calculations, transmission coefficients of all reaction paths are explicitly calculated and the M08-HX/6-31+G(d,p) potential energy surfaces are used. Notice that the two sets of results for R1c are not distinguishable on the plot because they are in excellent agreement.

Published on 29 February 2012 on http://pubs.rsc.org | doi:10.1039/C2FD20012K
Downloaded by University of Minnesota - Twin Cities on 20 January 2013

lowest-energy saddle points), and $\langle\gamma\rangle$ (averaged over all 14 reaction paths). At the low temperature of 200 K, $\langle\gamma\rangle_8$ and $\langle\gamma\rangle$ are very close because the sum of the weights of the eight lowest-energy paths is 94%, and the reaction is dominated by the reactive flux through these eight saddle points. The difference between $\langle\gamma\rangle_8$ and $\langle\gamma\rangle$ becomes larger at medium or high temperatures because the weight of those six highest-energy paths increase rapidly when temperature increases. For instance, the weight of the six highest-energy paths is 26% at 300 K, but it is 60% at 600 K. If we take the full path-averaged MP-VTST rate constants ($T = 200$–2400 K) as a benchmark for reaction R1b, the MS-VTST (based on γ_1 calculated using the lowest-energy path) rate constants have errors between 34% and 51%, and the MP-VTST rate constants using $\langle\gamma\rangle_8$ have errors between 4% and 22%.

The generalized transmission coefficients of the lowest-energy path of reaction R1c are very close to the averaged ones except at low temperatures. The difference between γ_1 and $\langle\gamma\rangle$ is about 20% to 13% in the range of temperature from 200 to 250 K because the two highest-energy paths have relatively large tunneling transmission coefficients, and the sum of the weights of these saddle points is 28%.

We plot the calculated branching fraction by the MS-VTST and the MP-VTST methods in Fig. 11. The R1a and R1b branching fractions obtained by the MS-VTST and the MP-VTST methods, respectively, differ by about 10%. The branching fractions for R1c are almost the same by the two methods. The branching fractions for R1a and R1b are in good agreement with a recent experiment[41] in both magnitude and temperature dependence over the entire 300–600 K temperature range of the measurement. The branching fraction for R1c has not been measured.[41]

IV. Concluding remarks

At this point we can recognize a hierarchy in the way that multiple structures and variational transition states are treated in various formulations of transition state theory. The most recent formulations, MS-VTST and MP-VTST (the latter formulated previously for unimolecular reactions and here for bimolecular ones), occupy an intermediate position between single-structure variational transition state theory[15,79,99], (called VTST, or, to emphasize the distinction, SS-VTST), which has been used very successfully for small molecules, and ensemble-averaged variational transition state theory[100–102] (EA-VTST), which has been used successfully for enzyme kinetics. EA-VTST is a multi-path method that could also be used for nonenzymatic reactions in solution, which can also be treated by single-path methods based on a potential of mean force.[19,25]

 This journal is © The Royal Society of Chemistry 2012

View Article Online

Based on the reactions studied in this work, the MS-VTST method that uses a transmission coefficient of a single reaction path to represent all reaction paths is sometimes a good approximation to the MP-VTST method in which the transmission coefficients of all reaction paths or of the most important paths are calculated explicitly. However, when a reaction has a set of saddle points that have diverse energies and geometries, the MP-VTST method with transmission coefficients averaged (with appropriate Boltzmann weighting) over all reaction paths or over the lowest-energy paths provides a better approach. More general conclusions on choosing the MS-VTST or the MP-VTST and on the strategies of choosing reaction paths will emerge as more diverse types of reactions are studied.

In general, one should be careful in viewing the agreement between experiment and theory in reaction rate calculations. The present study shows an example where agreement between theory and experimental data can be obtained by low-level calculations, while state-of-the-art theoretical methods lead to discrepancies. These discrepancies show that further development of both electronic structure theory and dynamics methods are needed to make reaction rate calculations more predictive.

Published on 29 February 2012 on http://pubs.rsc.org | doi:10.1039/C2FD20012K
Downloaded by University of Minnesota - Twin Cities on 20 January 2013

Acknowledgements

The authors are grateful to Rubén Meana-Pañeda, Antonio Fernández-Ramos, and John Alecu for constructive comments on a draft of the manuscript. This work was supported by the U. S. Department of Energy, Office of Basic Energy Sciences under grant no. DE-FG02-86ER13579 and by the Combustion Energy Frontier Research Center under award no. DE-SC0001198. Some of the computations were performed as part of a Computational Grand Challenge grant at the Molecular Science Computing Facility (MSCF) in the William R. Wiley Environmental Molecular Sciences Laboratory, a national scientific user facility sponsored by the U.S. Department of Energy's Office of Biological and Environmental Research and located at the Pacific Northwest National Laboratory, operated for the Department of Energy by Battelle.

References

1 J. Zheng, Y. Zhao and D. G. Truhlar, *J. Chem. Theory Comput.*, 2009, **5**, 808.
2 X. Xu, I. M. Alecu and D. G. Truhlar, *J. Chem. Theory Comput.*, 2011, **7**, 1667.
3 I. M. Alecu and D. G. Truhlar, *J. Phys. Chem. A*, 2011, **115**, 2811.
4 E. Wigner, *Trans. Faraday Soc.*, 1938, **34**, 29.
5 H. Eyring, *Trans. Faraday Soc.*, 1938, **34**, 41.
6 M. G. Evans, *Trans. Faraday Soc.*, 1938, **34**, 49.
7 M. Polanyi, *Trans. Faraday Soc.*, 1938, **34**, 75.
8 K. J. Laidler and M. J. King, *J. Phys. Chem.*, 1983, **87**, 2657.
9 D. G. Truhlar, W. L. Hase and J. T. Hynes, *J. Phys. Chem.*, 1983, **87**, 2664; D. G. Truhlar, W. L. Hase and J. T. Hynes, *J. Phys. Chem.*, 1983, **87**, 5523(E).
10 D. G. Truhlar, B. C. Garrett and S. J. Klippenstein, *J. Phys. Chem.*, 1996, **100**, 12771.
11 D. G. Truhlar and B. C. Garrett, *Annu. Rev. Phys. Chem.*, 1984, **35**, 159.
12 T. C. Allison and D. G. Truhlar, in *Modern Methods for Multidimensional Dynamics Computations in Chemistry*, ed. D. L. Thompson, World Scientific, Singapore, 1998, p. 618.
13 D. G. Truhlar, in *Isotope Effects in Chemistry and Biology*, edited by A. Kohen and H.-H. Limbach, Marcel Dekker, Inc., New York, 2006, p. 579.
14 B. C. Garrett and D. G. Truhlar, *J. Chem. Phys.*, 1979, **70**, 1593.
15 D. G. Truhlar and B. C. Garrett, *Acc. Chem. Res.*, 1980, **13**, 440.
16 D. G. Truhlar, A. D. Isaacson, R. T. Skodje and B. C. Garrett, *J. Phys. Chem.*, 1982, **86**, 2252; D. G. Truhlar, A. D. Isaacson, R. T. Skodje and B. C. Garrett, *J. Phys. Chem.*, 1983, **87**, 4554(E).
17 C. F. Jackels, Z. Gu and D. G. Truhlar, *J. Chem. Phys.*, 1995, **102**, 3188.
18 J. Villà and D. G. Truhlar, *Theor. Chem. Acc.*, 1997, **97**, 317.
19 Y.-Y. Chuang, C. J. Cramer and D. G. Truhlar, *Int. J. Quantum Chem.*, 1998, **70**, 887.
20 Y. Georgievskii and S. J. Klippenstein, *J. Chem. Phys.*, 2003, **118**, 5442.

View Article Online

21 Y. Georgievskii and S. J. Klippenstein, *J. Phys. Chem.*, 2003, **107**, 9776.
22 A. Fernández-Ramos, J. A. Miller, S. J. Klippenstein and D. G. Truhlar, *Chem. Rev.*, 2006, **106**, 4518.
23 J. Zheng, S. Zhang and D. G. Truhlar, *J. Phys. Chem. A*, 2008, **112**, 11509.
24 C. Alhambra, J. Corchado, M. L. Sánchez, M. Garcia-Viloca, J. Gao and D. G. Truhlar, *J. Phys. Chem. B*, 2001, **105**, 11326.
25 Y. Kim, J. R. Mohrig and D. G. Truhlar, *J. Am. Chem. Soc.*, 2010, **131**, 11071.
26 K. J. Laidler, *Chemical Kinetics*, 2nd ed., McGraw-Hill, New York, 1965, p. 72.
27 T. Yu, J. Zheng and D. G. Truhlar, *Chem. Sci.*, 2011, **2**, 2199.
28 T. Yu, J. Zheng and D. G. Truhlar, *J. Phys. Chem. A*, 2012, **116**, 297.
29 P. Seal, E. Papajak and D. G. Truhlar, *J. Phys. Chem. Lett.*, 2012, **3**, 264.
30 I. M. Alecu and D. G. Truhlar, *J. Phys. Chem. A*, 2011, **115**, 14599.
31 J. Zheng, R. J. Rocha, M. Pelegrini, L. F. A. Ferrão, E. F. V. Carvalho, O. Roberto-Neto, F. B. C. Machado and D. G. Truhlar, *J. Chem. Phys.*, 2012, **136**, 184310.
32 U. Meier, H. H. Grotheer, G. Riekert and T. Just, *Chem. Phys. Lett.*, 1985, **115**, 221.
33 U. Meier, H. H. Grotheer, G. Riekert and T. Just, *Chem. Phys. Lett.*, 1987, **133**, 162.
34 T. J. Wallington and M. J. Kurylo, *Int. J. Chem. Kinet.*, 1987, **19**, 1015.
35 W. P. Hess and F. P. Tully, *Chem. Phys. Lett.*, 1988, **152**, 183.
36 J. F. Bott and N. Cohen, *Int. J. Chem. Kinet.*, 1991, **23**, 1075.
37 E. Jimenez, M. K. Gilles and A. R. Ravishankara, *J. Photochem. Photobiol., A*, 2003, **157**, 237.
38 T. J. Dillon, D. Holscher, V. Sivakumaran, A. Horowitz and J. N. Crowley, *Phys. Chem. Chem. Phys.*, 2005, **7**, 349.
39 S. A. Carr, M. T. Baeza-Romero, M. A. Blitz, B. J. S. Price and P. W. Seakins, *Int. J. Chem. Kinet.*, 2008, **40**, 504.
40 R. Sivaramakrishnan, M. C. Su, J. V. Michael, S. J. Klippenstein, L. B. Harding and B. Ruscic, *J. Phys. Chem. A*, 2010, **114**, 9425.
41 S. A. Carr, M. A. Blitz and P. W. Seakins, *J. Phys. Chem. A*, 2011, **115**, 3335.
42 A. Galano, J. R. Alvarez-Idaboy, G. Bravo-Perez and M. E. Ruiz-Santoyo, *Phys. Chem. Chem. Phys.*, 2002, **4**, 4648.
43 S. Xu and M. C. Lin, *Proc. Combust. Inst.*, 2007, **31**, 159.
44 R. Atkinson, D. L. Baulch, R. A. Cox, J. N. Crowley, R. F. Hampson, R. G. Hynes, M. E. Jenkin, M. J. Rossi, J. Troe and IUPAC Subcommittee, *Atmos. Chem. Phys.*, 2006, **6**, 3625.
45 Y. Zhao and D. G. Truhlar, *J. Chem. Theory Comput.*, 2008, **4**, 1849.
46 Y. Zhao, N. E. Schultz and D. G. Truhlar, *J. Chem. Phys.*, 2005, **123**, 161103.
47 Y. Zhao and D. G. Truhlar, *Theor. Chem. Acc.*, 2008, **120**, 215.
48 J. Zheng, X. Xu and D. G. Truhlar, *Theor. Chem. Acc.*, 2011, **128**, 295.
49 K. Raghavachari, G. W. Trucks, J. A. Pople and M. Head-Gordon, *Chem. Phys. Lett.*, 1989, **157**, 479.
50 T. B. Adler, G. Knizia and H.-J. Werner, *J. Chem. Phys.*, 2007, **127**, 221106.
51 G. Knizia, T. B. Adler and H.-J. Werner, *J. Chem. Phys.*, 2009, **130**, 054104.
52 E. Papajak and D. G. Truhlar, *J. Chem. Theory Comput.*, 2011, **7**, 10.
53 S. Hirata, P.-D. Fan, A. A. Auer, M. Nooijen and P. Piecuch, *J. Chem. Phys.*, 2004, **121**, 12197.
54 E. Papajak, H. Leverentz, J. Zheng and G. T. Donald, *J. Chem. Theory Comput.*, 2009, **5**, 1197.
55 T. J. Lee and P. R. Taylor, *Int. J. Quantum Chem. Symp.*, 1989, **23**, 199.
56 J. C. Rienstra-Kiracofe, W. D. Allen and H. F. Schaefer III, *J. Phys. Chem. A*, 2000, **104**, 9823.
57 J. Peiró-García, I. Nebot-Gil and M. Merchán, *ChemPhysChem*, 2003, **4**, 366.
58 N. Lambert, N. Kaltsoyannis, S. D. Price, J. Žabka and Z. Herman, *J. Phys. Chem. A*, 2006, **110**, 2898.
59 I. M. Alecu, J. Zheng, Y. Zhao and D. G. Truhlar, *J. Chem. Theory Comput.*, 2010, **6**, 2872.
60 M. J. Frisch, G. W. Trucks, H. B. Schlegel, G. E. Scuseria, M. A. Robb, J. R. Cheeseman, G. Scalmani, V. Barone, B. Mennucci, G. A. Petersson, H. Nakatsuji, M. Caricato, X. Li, H. P. Hratchian, A. F. Izmaylov, J. Bloino, G. Zheng, J. L. Sonnenberg, M. Hada, M. Ehara, K. Toyota, R. Fukuda, J. Hasegawa, M. Ishida, T. Nakajima, Y. Honda, O. Kitao, H. Nakai, T. Vreven, J. A. Montgomery, Jr., J. E. Peralta, F. Ogliaro, M. Bearpark, J. J. Heyd, E. Brothers, K. N. Kudin, V. N. Staroverov, R. Kobayashi, J. Normand, K. Raghavachari, A. Rendell, J. C. Burant, S. S. Iyengar, J. Tomasi, M. Cossi, N. Rega, J. M. Millam, M. Klene, J. E. Knox, J. B. Cross, V. Bakken, C. Adamo, J. Jaramillo, R. Gomperts, R. E. Stratmann, O. Yazyev, A. J. Austin, R. Cammi, C. Pomelli, J. Ochterski, R. L. Martin, K. Morokuma, V. G. Zakrzewski,

Published on 29 February 2012 on http://pubs.rsc.org | doi:10.1039/C2FD20012K
Downloaded by University of Minnesota - Twin Cities on 20 January 2013

 This journal is © The Royal Society of Chemistry 2012

View Article Online

G. A. Voth, P. Salvador, J. J. Dannenberg, S. Dapprich, A. D. Daniels, Ö. Farkas, J. B. Foresman, J. V. Ortiz, J. Cioslowski and D. J. Fox, *GAUSSIAN 09 (Revision A.2)*, Gaussian, Inc., Wallingford, CT, 2009.
61 Y. Zhao, R. Peverati, K. Yang and D. G. Truhlar, *MN-GFM, version 5.1*, University of Minnesota, Minneapolis, 2011.
62 H.-J. Werner, P. J. Knowles, F. R. Manby, M. Schütz, P. Celani, G. Knizia, T. Korona, R. Lindh, A. Mitrushenkov, G. Rauhut, T. B. Adler, R. D. Amos, A. Bernhardsson, A. Berning, D. L. Cooper, M. J. O. Deegan, A. J. Dobbyn, F. Eckert, E. Goll, C. Hampel, A. Hesselmann, G. Hetzer, T. Hrenar, G. Jansen, C. Köppl, Y. Liu, A. W. Lloyd, R. A. Mata, A. J. May, S. J. McNicholas, W. Meyer, M. E. Mura, A. Nicklaß, P. Palmieri, K. Pflüger, R. Pitzer, M. Reiher, T. Shiozaki, H. Stoll, A. J. Stone, R. Tarroni, T. Thorsteinsson, M. Wang and A. Wolf, *MOLPRO*, University of Birmingham, Birmingham, *version 2010.1*, 2010.
63 M. Valiev, E. J. Bylaska, N. Govind, K. Kowalski, T. P. Straatsma, H. J. J. Van Dam, D. Wang, J. Nieplocha, E. Apra, T. L. Windus and W. A. de Jong, *Comput. Phys. Commun.*, 2010, **181**, 1477.
64 J. Zheng, T. Yu, E. Papajak, I. M. Alecu, S. L. Mielke and D. G. Truhlar, *Phys. Chem. Chem. Phys.*, 2011, **13**, 10885.
65 J. Zheng, S. L. Mielke, K. L. Clarkson and D. G. Truhlar, *Computer Phys. Comm.*, 2012, **183**, 1803.
66 J. Zheng, S. L. Mielke, K. L. Clarkson and D. G. Truhlar, *MSTor, version 2011–2*, University of Minnesota, Minneapolis, 2011.
67 D. G. Truhlar and A. Kuppermann, *J. Am. Chem. Soc.*, 1971, **93**, 1840.
68 Y.-P. Liu, G. C. Lynch, T. N. Truong, D.-h. Lu, D. G. Truhlar and B. C. Garrett, *J. Am. Chem. Soc.*, 1993, **115**, 2408.
69 D. K. Bondi, J. N. L. Connor, B. C. Garrett and D. G. Truhlar, *J. Chem. Phys.*, 1983, **78**, 5981.
70 M. M. Kreevoy, D. Ostović, D. G. Truhlar and B. C. Garrett, *J. Phys. Chem.*, 1986, **90**, 3766.
71 Y.-P. Liu, D.-h. Lu, A. Gonzàlez-Lafont, D. G. Truhlar and B. C. Garrett, *J. Am. Chem. Soc.*, 1993, **115**, 7806.
72 A. Fernandez-Ramos and D. G. Truhlar, *J. Chem. Phys.*, 2001, **114**, 1491.
73 B. C. Garrett and D. G. Truhlar, *J. Chem. Phys.*, 1983, **79**, 4931.
74 R. Meana Pañeda, D. G. Truhlar and A. Fernández-Ramos, *J. Chem. Theory Comput.*, 2010, **6**, 6.
75 B. C. Garrett, D. G. Truhlar, R. S. Grev and A. W. Magnuson, *J. Phys. Chem.*, 1983, **84**, 1730; B. C. Garrett, D. G. Truhlar, R. S. Grev and A. W. Magnuson, *J. Phys. Chem.*, 1983, **87**, 4554 (E).
76 D. G. Truhlar, A. D. Isaacson and B. C. Garrett, in *Theory of Chemical Reaction Dynamics*, ed. M. Baer (CRC Press, Boca Raton, FL, 1985), Vol. 4, pp. 65–137.
77 A. Fernández-Ramos, B. A. Ellingson, B. C. Garrett and D. G. Truhlar, *Rev. Comput. Chem.*, 2007, **23**, 125.
78 A. Fernández-Ramos, B. A. Ellingson, R. Meana-Pañeda, J. M. C. Marques and D. G. Truhlar, *Theor. Chem. Acc.*, 2007, **118**, 813.
79 A. Fernandez-Ramos, B. A. Ellingson, B. C. Garrett and D. G. Truhlar, *Rev. Comput. Chem.*, 2007, **23**, 125.
80 J. Zheng, S. Zhang, B. J. Lynch, J. C. Corchado, Y.-Y. Chuang, P. L. Fast, W.-P. Hu, Y.-P. Liu, G. C. Lynch, K. A. Nguyen, C. F. Jackels, A. F. Ramos, B. A. Ellingson, V. S. Melissas, J. Villà, I. Rossi, E. L. Coitino, J. Pu, T. V. Albu, R. Steckler, B. C. Garrett, A. D. Isaacson and D. G. Truhlar, *POLYRATE, version 2010-A*, University of Minnesota, Minneapolis, 2010.
81 J. Villà and D. G. Truhlar, *Theor. Chem. Acc.*, 1997, **97**, 317.
82 R. K. Boyd, *Chem. Rev.*, 1977, **77**, 93.
83 M. M. Kreevoy and D. G. Truhlar, *Tech. Chem. (N.Y.)*, 4th edn, 1986, **6/Pt. 1**, 13.
84 J. B. Anderson, *Adv. Chem. Phys.*, 1995, **91**, 381.
85 S. Winstein and N. J. Holness, *J. Am. Chem. Soc.*, 1955, **77**, 5562.
86 J. E. Baldwin, A. S. Raghavan, B. A. Hess and L. Smentek, *J. Am. Chem. Soc.*, 2006, **128**, 14854.
87 R. Meana-Pañeda and A. Fernández-Ramos, *J. Am. Chem. Soc.*, 2012, **134**, 346.
88 J. E. Seeman, *J. Chem. Educ.*, 1986, **63**, 42.
89 B. C. Garrett and D. G. Truhlar, *J. Phys. Chem.*, 1980, **84**, 805.
90 P. Pechukas, *Annu. Rev. Phys. Chem.*, 1981, **32**, 159.
91 A. D. Isaacson, M. T. Sund, S. N. Rai and D. G. Truhlar, *J. Chem. Phys.*, 1985, **82**, 1338.
92 L. F. Phillips, *J. Chem. Phys.*, 1990, **92**, 6523.
93 F. T. Smith, *Discuss. Faraday Soc.*, 1962, **33**, 183.

Published on 29 February 2012 on http://pubs.rsc.org | doi:10.1039/C2FD20012K
Downloaded by University of Minnesota - Twin Cities on 20 January 2013

View Article Online

94 V. Bernshtein and I. Oref, *J. Phys. Chem. A*, 2004, **108**, 8131.
95 A. Galano, M. Francisco-Marquez and J. R. Alvarez-Idaboy, *J. Phys. Chem. B*, 2011, **115**, 8590.
96 K. A. Nguyen, C. F. Jackels and D. G. Truhlar, *J. Chem. Phys.*, 1996, **104**, 6491.
97 J. Zheng and D. G. Truhlar, *Phys. Chem. Chem. Phys.*, 2010, **12**, 7782.
98 P. S. Zuev, R. S. Sheridan, T. V. Albu, D. G. Truhlar, D. A. Hrovat and W. T. Borden, *Science*, 2003, **299**, 867.
99 B. C. Garrett and D. G. Truhlar, *J. Chem. Phys.*, 1979, **70**, 1593.
100 C. Alhambra, J. Corchado, M. L. Sánchez, M. Garcia-Viloca, J. Gao and D. G. Truhlar, *J. Phys. Chem. B*, 2001, **105**, 11326.
101 D. G. Truhlar, J. Gao, C. Alhambra, M. Garcia-Viloca, J. Corchado, M. L. Sánchez and J. Villà, *Acc. Chem. Res.*, 2002, **35**, 341.
102 D. G. Truhlar, J. Gao, M. Garcia-Viloca, C. Alhambra, J. Corchado, M. L. Sanchez and T. D. Poulsen, *Int. J. Quantum Chem.*, 2004, **100**, 1136.

Published on 29 February 2012 on http://pubs.rsc.org | doi:10.1039/C2FD20012K
Downloaded by University of Minnesota - Twin Cities on 20 January 2013

 This journal is © The Royal Society of Chemistry 2012